POTENTIAL OF HIGH-TEMPERATURE SUPERCONDUCTORS FOR SHORT-TERM MICROWAVE APPLICATIONS

MATTHIAS A. HEIN

Dept. of Physics, Univ. of Wuppertal, Gaußstraße 20, 42097 Wuppertal, Germany

The four preceding workshops on RF superconductivity have witnessed an extraordinary rapid development of the technology of the high-temperature superconductors (HTS). Up to 40 different HTS compounds have been successfully synthesized by different physical and chemical evaporation and ablation techniques. Ingenious methods to characterize the temperature, frequency and power dependent surface impedance Z_s and to optimize the material have been developed and thoroughly adopted. Although some fundamental physics questions are still puzzling, many possible applications of planar microwave components have been identified which utilize epitaxial HTS thin films at frequencies between 1 MHz and 100 GHz. These can be devided into passive or active, based on the linear or the nonlinear dynamic conductivity of HTS, and analog or digital. This review tries to summarize the present phenomenological understanding of Z_s of the HTS compounds $YBa_2Cu_3O_{7-x}$ and $Tl_2Ba_2CaCu_2O_{8+y}$, its short-term impact on different categories of microwave circuit components and the resulting technical and economical potentials for implementing such HTS devices in operational high-frequency systems.

1 INTRODUCTION

The discovery of the high-temperature superconductors has dramatically influenced recent research activities and is yet attracting increasing attention from scientists as well as economists. Chemists, physicists and material engineers have merged their interests in order to develop a comprehensive understanding and a consequent exploitation of the wide-spread potential that these novel compounds promise. Since the discovery of HTS, enormous technological improvements in the preparation and physical characterization of high-quality epitaxial HTS films have been achieved. Moreover, considerable progress has been attained meanwhile in the design, fabrication and functional demonstration of single microwave components and more complicated subsystems, which significantly benefit from utilizing HTS. Several books and extended articles were devoted to the application of HTS in high-frequency systems, as discussed in some recent reviews[1,2]. Potential customers have become aware of promising market opportunities, and tremendous efforts are currently aiming at the commercialization of HTS systems in communication and remote sensing systems[3,4].

This review is the fifth contribution in a row of workshops on RF superconductivity, which aimed at describing the impact of HTS to this challenging field. With respect to the layered structure of these novel materials, realistic applications cover analog microwave devices composed of cm^2-large planar superconductive elements rather than high-field gradient accelerating systems extending over complex-shaped m^2-surfaces. The paper intends to sketch from a general point of view basic physical and technological features underlying the present state-of-the-art, and remaining to be addressed before successful commercialization. The reviewed examples represent selected contributions and should not be expected to be complete in every regard.

In Sec. 2, fundamental physical issues for microwave applications of HTS are summarized. The extremely large Ginsburg-Landau parameter ($\kappa_{GL} \geq 100$), the pronounced

anisotropy and the unusual electronic phase diagram are the basic features determining their transport properties. Reflecting the potential for realistic microwave applications of HTS, the review will be focused on the $YBa_2Cu_3O_{7-x}$ (Y-123) and $Tl_2Ba_2CaCu_2O_y$ (Tl-2212) superconductors and on frequencies between 10^{-3} and 10^2 GHz. Recent developments of refrigeration techniques are, according to their importance for operational microwave systems, outlined in Sec. 3. Microwave components, based on linear and nonlinear conductivity properties of HTS, which are of major interest for short-term applications, are discussed in Sec. 4. A supplementary analysis of active elements and digital devices can be found, e. g., in Ref. 2. The paper is concluded in Sec. 5 by evaluating future prospects of HTS in terms of system aspects and related projections of the future market development.

2 SURFACE IMPEDANCE OF HTS: PHENOMENOLOGICAL DESCRIPTION

2.1 Two-fluid model of the surface impedance

The interaction between high-frequency fields and superconductors is determined by the surface impedance Z_s. Its real part, the surface resistance R_s, characterizes the dissipated microwave power per unit surface area, $\partial P/\partial A=1/2\cdot R_s\cdot H_s^2$, with H_s the microwave magnetic surface field. The imaginary part of Z_s, the surface reactance $X_s=\omega\mu_0\lambda$, describes the non-dissipative energy exchange between the microwave field and the superconductor within the penetration depth λ. For isotropic low-temperature superconductors (LTS), Z_s can be calculated as a function of operating frequency $\omega=2\pi f$ and temperature T by means of weak-[5] or strong-coupling microscopic theories[6]. The calculation of Z_s of HTS is, compared to LTS, much more complicated because of the high critical temperatures, the strong electronic anisotropy and the possible relevance of unconventional pairing mechanisms (see, e. g., Ref. 2 and below) .

A valuable access towards a comprehensive description of the microwave properties of HTS is attained by parametrizing the material properties with the complex conductivity $\sigma=\sigma_1-i\sigma_2$[7,8]:

$$Z_s = R_s - iX_s = \left(\frac{\mu_0\omega}{\sigma_1 - i\sigma_2}\right)^{1/2} \qquad (1)$$

The validity of Eq. (1) is restricted to the local limit, where the scale of spatial variation of the magnetic fields (λ) significantly exceeds the ranges of the pair- (ξ) and the quasiparticle interaction (l). Within the framework of the two-fluid model[9], σ_1 and σ_2 are related to the number densities of the (un-) paired charge carriers, n_N and n_S. While an approved theoretical description for HTS is still lacking, σ_1 may be reasonably well approached by a simple Drude model, i. e. assuming a frequency independent quasiparticle scattering time[10] τ:

$$\sigma(\omega,T) = \frac{n_e e^2}{m}\left(\frac{x_N\cdot\tau(T)}{1-i\omega\tau(T)} - i\frac{x_S}{\omega}\right) \qquad (2)$$

with $x_N=n_N/n_e$, $x_S=2n_S/n_e$ and n_e the total number density of charge carriers. The normal conductivity $\sigma_1=\mathrm{Re}(\sigma)$ at $\omega>0$ depends on the effective mass and the scattering rate $\tau^{-1}=v_F/l$ of the quasiparticles. The inductive response is described by $\sigma_2=\mathrm{Im}(\sigma)$ which, for $\omega\tau<<1$ and $x_N<<x_S$, is given by $1/\mu_o\omega\lambda^2$ where $\lambda(T=0K)=\lambda_L$. Combining Eqs. (1) and (2), Z_s can be expressed in terms of σ_1 and the dimensionless conductivity ratio[2] $y\equiv\sigma_1/\sigma_2$:

$$Z_s = \left(\frac{\mu_0\omega}{2\sigma_1}\right)^{1/2} \cdot (\varphi_- - i\varphi_+) \text{ with } \varphi_\pm^2 = \frac{y}{1+y^2}\{(1+y^2)^{1/2} \pm 1\} \quad (3)$$

Eq. (3) reduces in the limit $y<<1$ to the well known result $R_s=1/2\mu_0^2\omega^2\sigma_1\lambda^3$. Within the two-fluid model, the lumped-element representation of a superconductor[11] consists of a resistivity, $\rho=1/\sigma_1$, shunted inductively by $l_{kin}=1/\omega\sigma_2$. At T=0 and $\omega\tau<<1$, l_{kin}=0.18 pHm results for λ_L=140 nm. With $\omega\tau$ approaching unity, quasiparticle retardation leads to additional shielding causing a reduced $\lambda_{eff}(T)=(\mu_0\omega\sigma_2)^{-1/2}$. Tunneling, infrared and microwave spectroscopy yielded highly temperature dependent quasiparticle scattering rates between T_c and 4.2 K between 0.1 to 10 THz (cf. Refs. 10,12,13,14 and Sec. 2.2.1). Since τ^{-1}=1 THz corresponds to a mean free path of l≈100 nm, which is of the order of λ_L, the validity of Eq. (3) (i. e. the local response to electromagnetic fields) becomes questionable at low temperatures. For ω approaching the gap frequency of the superconductor Δ/h, and for non-vanishing[15] x_N, σ_1 increases while σ_2 decreases. As y approaches 1, the surface impedance reaches the normal value $R_s=X_s=\omega\mu_0\sigma_1^{-1/2}/2$.

As indicated by Eqs. (1) to (3), the transport properties of HTS are determined solely by x_N since x_S is given by $1-x_N$. The fraction x_N of quasiparticles sensing the microwave field is given by the density of quasiparticle states N(E) in the superconductor, which is fundamentally determined by the energy gap Δ. For HTS, especially for the Bi:Sr:Ca:Cu:O-2:2:1:2:(8-x) (Bi-2212) and 2:2:2:3:(10-x) and the Y-123 compounds, there is strong evidence from electron tunneling and photon emission spectroscopy for the existence of a large energy gap, Δ=25-30 meV, and a short quasiparticle lifetime, $\Gamma/\Delta\geq0.1$[13,16,17,18,19]. The reported gap energies correspond to reduced values $\alpha=2\Delta/kT_c\approx$5-7 indicating a strong pair coupling. These large values imply an enormous potential benefit of HTS compared to LTS in terms of reduced thermal sensitivity ($\Delta/k\approx10^2$K), very short dynamic response times ($h/\Delta\approx$0.1ps) and high operation frequencies ($\Delta/h\approx$10THz).

Besides the absolute value of Δ, its isotropy and multiplicity also affect the high-frequency transport properties. Knowledge of these features is therefore crucial for proper material and device engineering. Angle-resolved photo emission spectroscopy gave clear evidence of a pronounced gap anisotropy within the CuO_2 planes of the HTS compounds [17,18]. Data on tunneling and microwave spectroscopy have revealed the coexistence of two distinct gap features[10,16,20,21] with Δ_1=25-30 meV, $\Delta_2\leq$10 meV or α_1=5-7 and $\alpha_2\leq$2. Assuming a conventional pairing mechanism, i. e. $x_N(T)\propto\exp(-\alpha_i/2t)$ for i=1,2, the smaller gap will dictate the temperature dependence of x_N and thus of R_s at low temperatures.

2.2 Phenomenology of the high-frequency properties of HTS

There are many different methods to deduce the surface impedance in terms of its real and imaginary parts, R_s and X_s, from experiment (e. g. from the unloaded quality factor and the resonant frequency of a microwave resonator), which were already reviewed in great details[1,22,23,24] and will therefore not be described here. To extract the equivalent surface impedance of infinitely thick superconductors, effectively enhanced values of Z_s of thin films must be corrected for the finite film thickness[25] $d/\lambda\leq1$.

The high-frequency properties of HTS single-crystals and epitaxial films prepared by many different techniques (e. g., sputtering, pulsed laser deposition and physical or chemical evaporation techniques) have also been subject of numerous publications (e. g., Refs. 1,22,24 and Refs. therein). Since very high quality films can be obtained by each

of these techniques, only general features are summarized in the following, the analysis being restricted to the Y-123 and Tl-2212 compounds. Besides the absolute values of the surface impedance, its dependences on external parameters affect the performance of microwave devices. The surface resistance determines parameters like the quality factor of resonators or, in other terms, the bandwidth and the skirts of filter elements, the radiation efficiency of antennas and the insertion loss of transmission lines. Analogously, the surface reactance affects, e. g., the center frequency of resonant structures, the energy stored in the near field of radiation elements and the kinetic inductance, the propagation velocity and the dispersion of transmission line elements (Sec. 4.1).

2.2.1 Temperature dependence of the surface impedance Figs. 1a and 2 display typical temperature dependences of the surface resistance on linear scales as obtained for a Y-123 single-crystal[10] and in an Arrhenius plot as obtained for very high quality Y-123 thin films[21]. From both figures, three different temperature regimes can be distinguished.

Close to T_c, the steep decrease of R_s under cooling results from the field expulsion as the microwave penetration depth reduces from the normal skin depth λ_N to the superconductor penetration depth λ. Within the two-fluid model, the ratio of the penetration depths λ/λ_N scales with temperature and frequency as $y^{1/2}$.

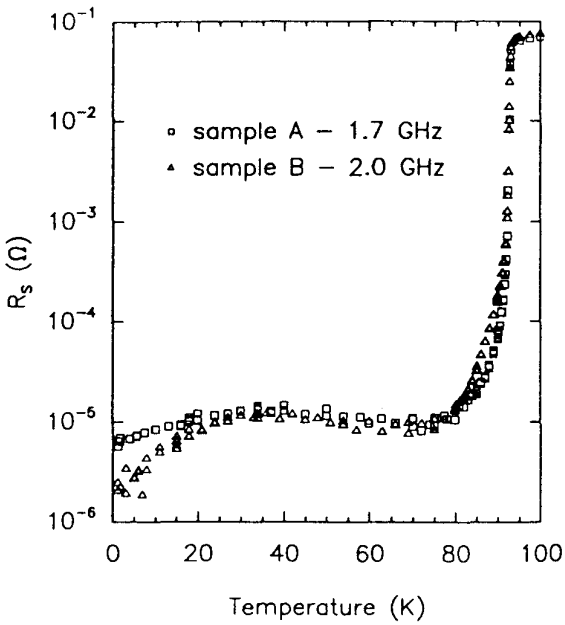

Fig. 1a: Temperature dependence of the surface resistance of two different Y-123 single-crystals[10].

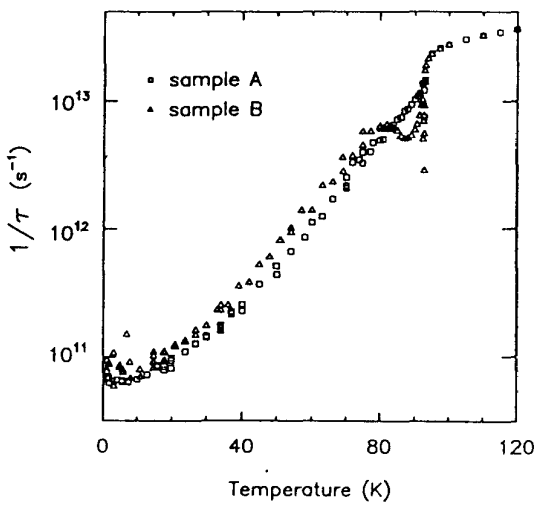

Fig. 1b: Temperature dependence of the quasi-particle scattering rate extracted from the data in Fig. 6a assuming that the spectral shape of the quasiparticles is Drude-like[10].

In the temperature range $t \leq 0.8$, a non-monotonic behavior in $R_s(T)$ is often observed for high-quality samples. At a temperature T_0, which increases with increasing frequency ($T_0 \approx 30$ K at 2 GHz[10], 40 to 50 K at 8 GHz[26], 50 K at 87 GHz[21] and 70 K at 600 GHz[12]), R_s passes through a broad maximum. This behavior was attributed in Ref. 10 to a strongly temperature dependent scattering rate, which leads to the superposition of two opposite effects: while x_N decreases with decreasing temperature, τ increases and causes the observed maximum (Eq. (3)). Fig. 1b displays the results for σ_1 which were correspondingly deduced from the data in Fig. 1a[10].

At even lower temperatures, $t \leq T_0/T_c$, the surface resistance is dominated by either residual losses or by the existence of a small gap. Experimental observation of an exponential $R_s(T)$ dependence at $t<1/2$ with a small reduced energy gap of $\alpha_2=0.4$ was reported for sputtered Y-123 films[27]. Such a behavior was found only for well oxygenated samples which were post-annealed and slowly cooled in plasma-activated oxygen. The exponential $R_s(T)$ disappeared after a few days, presumably due to oxygen loss. Further support for two-gap superconductivity in Y-123 films was reported in Refs. 20,28,29,30 for different films and single-crystals. The data in Fig. 2 yielded reduced energy gap values of $\alpha=1.4$-1.6 after a residual resistance of about 1 mΩ was subtracted. Also shown are data on Nb samples which can be quantitatively described within BCS formalism with $\alpha=3.57$.

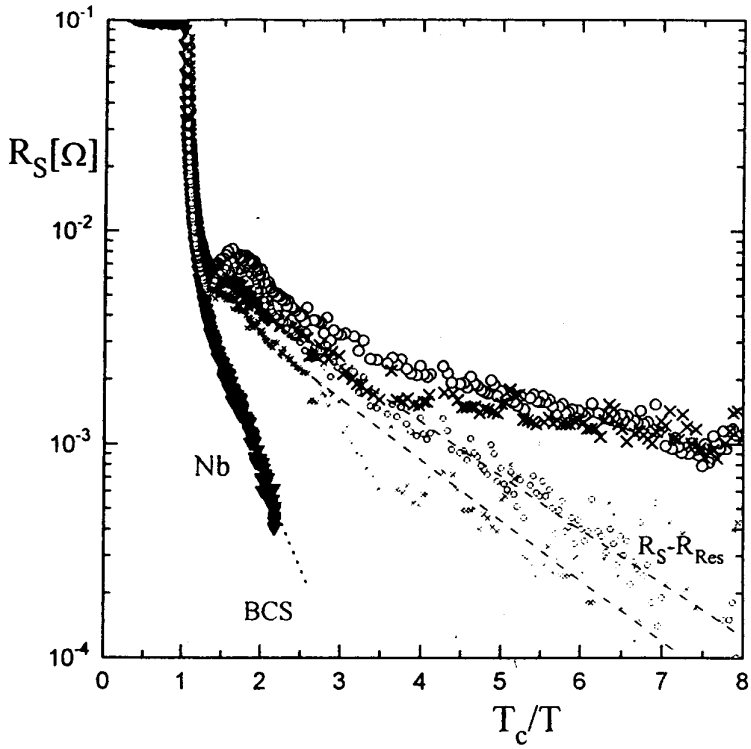

Fig. 2: Temperature dependence of log(R_s) at 87 GHz of two high-quality Y-123 films[21], plotted versus the inverse reduced temperature, as-measured (bold symbols) and after subtraction of the residual value of R_s (thin symbols and dashed lines). Data on a Nb sample are shown for comparison.

A remarkable effect of oxygen deficiency and disorder on the low-temperature behavior of R_s of Y-123 films at 87 GHz was reported in Ref. 30. The microwave losses displayed a strong reversible dependence on post-annealing the films. An almost temperature independent R_{res} of 70 mΩ was found after quench cooling (<20 s), but a much smaller R_s(20 K) of only a few mΩ after slow cooling (<1 h) of the same film, even after reducing its oxygen content (T_c=80 K). This observation was interpreted in terms of a two-gap model[31] by assuming that the different levels of oxygenation led to different values of the Cu-O chain gap. The effect of different metal stoichiometries of coevaporated Y-123 films on R_s(87 GHz) was analyzed in Ref. 32. Only a slight variation of R_s was found within 2% of cation variation around the optimum 1-2-3 composition. Parasitic effects resulted from different oxygenation levels and, possibly, different

scattering rates. In fact, the different morphologies observed for films of different compositions were supposed to affect R_s dominantly by different conditions for oxygen diffusion[21,33]. The analysis revealed $R_s(T)$ to be determined mainly by oxygen stoichiometry and order rather than by granular effects.

In contrast to LTS, even the best epitaxially grown Y-123 films exhibit a large residual surface resistance R_{res} (Fig. 2 and Refs. 22,24). While the lowest measured R_{res}-values for Nb and Nb_3Sn at t=0.2 stay in the nΩ range up to frequencies of 20 GHz ($hf/\Delta \approx 3\%$ and 1.3%, respectively), R_{res}-values at 20 K of only about 20 (1000) μΩ at 10 (87) GHz[14,21,34,35] have been obtained reproducibly for Y-123. As pointed out in Ref. 2, this high residual level seems to result from extrinsic rather than intrinsic loss mechanisms. Estimations of R_s from surface impedance calculations on the basis of the BCS theory for isotropic superconductors using material parameters for currents in the CuO_2 planes result in R_s(10 GHz, 20 K)≈10 nΩ[36]. These calculations demonstrated that the advantage of a larger gap frequency in HTS is partially compensated by the larger ratio λ/ξ. More realistic R_s-values result from the two-gap model[31]. A small or even vanishing value of the energy gap Δ_2, which is to be associated with the Cu-O-chains, leads to an enhanced value of x_N and hence of R_s. The predicted sensitivity of Δ_2 on content and order of the chain-oxygen agrees with the experimental situation: a much stronger spread is observed in R_s at 20 K than at 77 K[37]. For d-wave superconductors, a limiting value for R_{res} is also expected, which results from a minimum obtainable conductivity[38,39,40] $\sigma_{1,min}$, which is limited by the reduced scattering rate[2]: $\sigma_{1,min}/\sigma_1(t\geq 1) \approx \Gamma(0)/\Delta(0) \leq 0.2$[19,38]. Using $\lambda(0)$=140 nm and Eq. (3) in the limit $y \ll 1$ one obtains $R_{s,min} \approx 1$ μΩ at 10 GHz, which is about one order of magnitude below the majority of measured values.

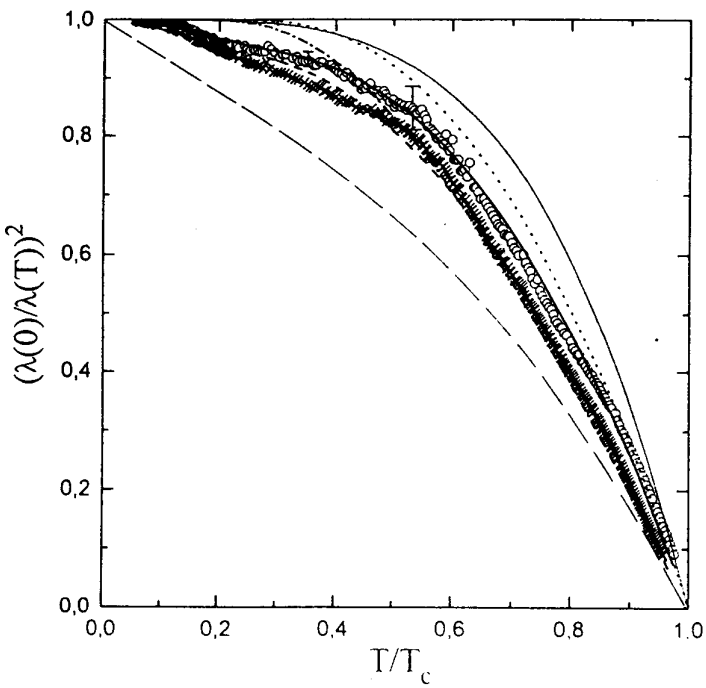

Fig. 3: Temperature dependence at 87 GHz of the inverse squared penetration depth, normalized to its low-temperature value, for the two Y-123 films of Fig. 2[21]. Also shown are the results expected for the two-fluid model (thin solid curve), a weakly (dash-dotted) and strongly coupled (dotted) isotropic single-gap BCS-like and a strongly coupled d-wave superconductor[41](coarsely dashed). The bold solid and dashed curves are fits to the two-gap model[42] with $\lambda(0)$=160 nm and α_1=5 (4), α_2=1 (0.5) for the two films.

Fig. 3 displays the results on the temperature dependence of the microwave penetration depth obtained for the two films[21] of Fig. 2. The inverse squared penetration depth, normalized to its value at zero-temperature, is plotted versus reduced temperature. According to the two-fluid formalism, this value equals x_s. The usual scaling $x_s=1-t^4$ is represented by the thin solid curve. The results for weakly and strongly coupled isotropic single-gap BCS-like superconductors are given by the dash-dotted and dotted curves. In contrast, the measured $x_s(t)$ displays a much weaker (stronger) temperature dependence at $t<<1$ ($t\approx1$). Such a behavior was found also by other authors[14,34] and interpreted as indications for d-wave superconductivity. The calculations[41] for a strongly coupled d-wave superconductor (cubic $d_{x^2+y^2-z^2}$-symmetry, vector potential $\underline{A}$ parallel to the principal axis of the gap symmetry, $\underline{G}$) are also given in the figure (long-dashed). The case $\underline{A}\perp\underline{G}$ and the results for weak coupling and tetragonal $d_{x^2-y^2}$-symmetry show similar or even worse deviations from the experimental data. Finally, the bold solid and dashed curves represent calculations of $x_s(t)$ within the two-gap s-wave approach[42]. The data can be quantitatively described over the complete temperature range using $\lambda(0)=160$ nm and $\alpha_1=5$ (4) and $\alpha_2=1$ (0.5) as fit parameters for the two films. Except for the change in slope of x_s at $t\approx0.5$, the data are consistent with an empirical power-law $x_s(t)=1-t^2$. Such a scaling was found in Refs. 10, 43 as a general feature describing many different λ-measurements for Y-123. The low-temperature value of the penetration depth was found to vary monotonously with oxygen content[33].

2.2.2 Frequency dependence of the surface impedance Knowledge of the frequency dependence of the surface impedance is crucial for microwave applications of HTS. Fig. 4 is a double-logarithmic plot of R_s versus frequency[21] depicting selected data on high-quality Y-123 at T=77 K. The advantage of single-crystals (crosses) and epitaxial films (bulk symbols) compared to copper or polycrystalline Y-123 (open symbols) is clearly resolved. Y-123 displays a lower surface resistance than copper up to about 200 GHz. Data on Tl-2212 fall at 77 K about a factor of 2 below the data on single-crystalline Y-123 due to the high T_c of 106 K[44]. The overall trend of $R_s(f)$ of HTS resembles that of the conventional superconductors Nb and Nb_3Sn.

Care has to be taken in scaling the surface resistance of HTS generally quadratic in frequency. As shown earlier, the frequency exponent b in the power-law $R_s\propto f^b$ can be calculated consistently within the two-fluid approach(cf. Eq. (3))[45]:

$$b = 1 + \frac{y^2}{2(1+y^2)} \cdot \{\frac{1}{1-(1+y^2)^{-1/2}} - 2\} \qquad (4)$$

According to this analysis, deviations from b=2 result from a finite value of the conductivity ratio $y=\sigma_1/\sigma_2\propto\omega/\rho$, and are thus expected to depend on the absolute values of frequency and normal-state resistivity. In the limit $y>>1$, Eq. (4) yields b=1/2 in accordance with the normal skin effect. In the opposite limit, b approaches 2 like $b=2-y^2$. The frequency dependence of b agrees well with the data in Fig. 4, leading to $b\approx2$, 1.92 and 1.68 at 10, 50 and 100 GHz, respectively. The measured dependence of b on the normal-state resistivity ρ of high-quality epitaxial films[21] at 77 K is displayed in Fig. 5. Using b=1.5 at f=87 GHz, T=77 K and $\rho=50$ $\mu\Omega$cm results in the empirical formula

$$b \approx 2 - 0.165 \cdot \{\frac{f[\mathrm{GHz}]}{\rho[\mu\Omega\mathrm{cm}]}\}^2 \qquad (5)$$

which quantitatively reproduces the data in Figs. 4 and 5.

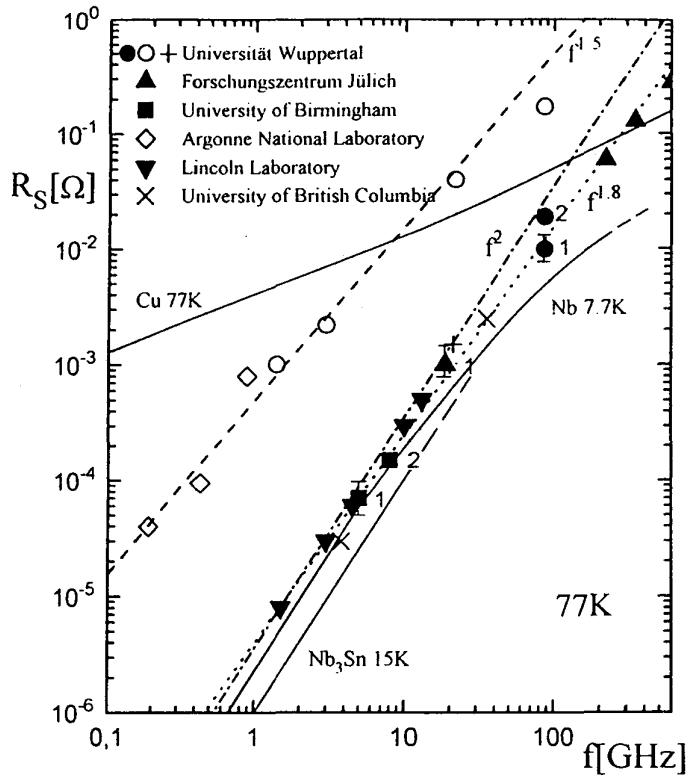

Fig. 4: Frequency dependence of R_s(77 K) of high-quality Y-123 single crystals (crosses) and epitaxial films (filled symbols) compared to polycrystalline samples (open symbols) and Cu. Data on Nb and Nb_3Sn are given at corresponding reduced temperatures[21].

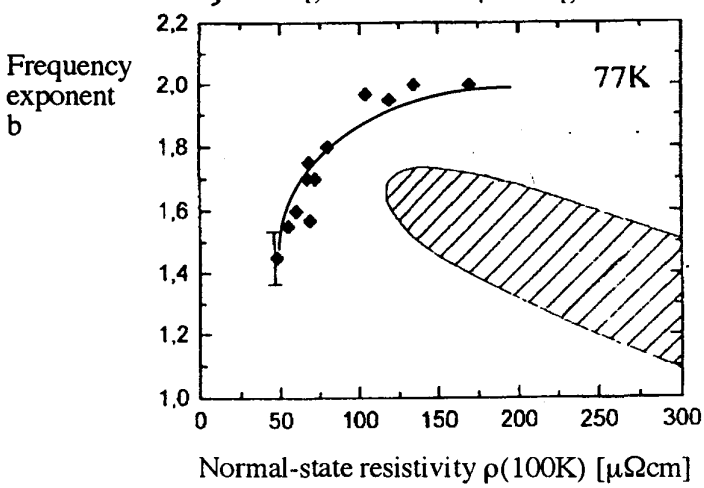

Fig. 5: Dependence of the frequency exponent $b=\partial(\log R_s)/\partial(\log f)$ on the normal-state resistivity, measured at 87 GHz for epitaxial Y-123 films (diamonds)[21]. The solid line represents the empirical formula given in Eq. (5). The results obtained with granular thick films[45] at 21 GHz are indicated by the shaded area.

As can be seen from Fig. 5, the b(ρ)-dependence of polycrystalline thick films deviates significantly from that of epitaxial thin films. Enhanced resistivity values result from the presence of weakly superconducting grain boundaries which, in turn, suppress the frequency exponent. In contrast, for epitaxial films, b is mainly affected by unpaired

charge carriers in the superconducting grains themselves. This conclusion follows directly from the two-fluid interpretation and indicates granular effects to be negligible.

In order to analyze the temperature dependence of b, Eq. (4) needs to be supplemented, according to Sec. 2.1, by:

$$y = \frac{x_N(\omega,t)\cdot\omega\tau(t)}{1-x_N(\omega,t)+\{\omega\tau(t)\}^2} \tag{6}$$

Since scattering effects depend sensitively on the crystalline quality of the films, no general prediction can be deduced for b(t). Experimental results[21] on epitaxial films at 87 GHz indicate shallow changes of $|b(0.8T_c)-b(4.2K)|\leq 0.3$.

Regarding the use of HTS for dispersive microwave devices, the frequency dependence of the effective microwave penetration depth has to be considered. Referring again to Eq. (3) (where the normal conductivtiy is assumed Drude-like), λ_{eff} is given by:

$$\frac{\lambda_L(t)}{\lambda_{eff}(\omega,t)} = \left[1-\frac{x_N(\omega,t)}{1+\{\omega\tau(t)\}^2}\right]^{1/2} \tag{7}$$

Considering typical data[2] on $\tau(t)$ and $x_N(\omega,t)$, deviations of λ_{eff} from $\lambda_L(t)$ have to be expected at temperatures $t\leq 0.5$ in a frequency range between 10 and 100 GHz or at frequencies above 300 GHz.

2.2.3 Magnetic field dependence of the surface impedance Besides temperature and frequency, magnetic field presents a key parameter affecting the surface impedance of superconductors. While a low-frequency magnetic field (or flux density) causes significant increases in R_s and X_s only above the lower critical field B_{c1}, high-frequency fields display a more complicated behavior due to the different time scale that such fields are probing. The lower critical field of Y-123 was found to be about 25 (50-90) mT at 4.2 K for shielding currents within (perpendicular to) the CuO_2 planes[46,47,48]. The surface impedance of HTS in the mixed state has been investigated by many groups (see reviews[11,49] and more recent work[50,51,52,53]). Since most of the microwave applications discussed later are restricted to weak external dc fields $B_{dc}<B_{c1}$, the behavior of $Z_s(B_{dc})$ will not be discussed further. It shall only be noted that HTS in the mixed state exhibit characteristic time scales of the order of $(10\ GHz)^{-1}$ and that $Z_s(B_{dc})$ provides valuable insight into their complicated magnetic phase diagram.

The effect of a high-frequency field of amplitude B_{rf} on the surface impedance is physically related, though not always equivalent, to the effect of an alternating current density of amplitude J_{rf}. Two different regimes can roughly be distinguished for $Z_s(B_{rf})$: linear behavior at field strengths below a certain limit, $B_{rf}<B_{cr}$, where R_s and X_s are constant, and nonlinear behavior at $B_{rf}>B_{cr}$, where R_s and X_s vary as B_{rf}^c, $c>1$. As long as the power-induced nonlinear loss mechansims depend only on the amplitude and not on the sign of the excitation, the general behavior is expected to be:

$$R_s(b_{rf})=A_1+A_2\cdot b_{rf}^2+A_3\cdot b_{rf}^4+\ldots \tag{8}$$

where b_{rf} is the rf field level normalized to an appropriate scaling field like, e. g., B_{cr}. The linear regime ($A_2=A_3=0$) is of crucial importance for the construction of devices which need to sustain high microwave field levels with optimum performance (Secs. 4.2 and 4.3). In this case, the crossover field B_{cr} should be as high as possible. B_{rf} denotes a local maximum rather than an average, which can be numerically derived for given boundary conditions. Compared to unpatterned films or cavity resonators, B_{rf} takes enhanced values at the signal lines of patterned devices, e. g., in coplanar, stripline or microstrip configu-

rations. Additional field enhancement at the edges of these lines may result from the geometric dimensions of such devices. In the opposite case, nonlinear effects (e. g., $A_2>>A_1$ in Eq. (8)) may be desired for special types of signal processing (Sec. 4.4). The nonlinear phenomena need to be understood or at least reproducible and empirically controllable in order to optimize either type of applications.

Nonlinear microwave properties in HTS have most commonly been studied by investigating the power dependence of the surface impedance of unpatterned or patterned films. Other, and more sensitive, methodes can be applied as well, which also address more realistically the performance issues of useful devices. These can be distinguished from the multiplicity, the power level and the modulation of the driving signal(s). Five different types have been summarized in Ref. 54: harmonic generation, intermodulation, saturation and desensitization, cross modulation and conversion of amplitude- to phase-modulation. In addition, nonlinear effects can be studied either in the frequency-domain or in the time-domain where the dynamic response of the test objects to excitation pulses of variable amplitude and duration is investigated. Many of these methods have been applied to study nonlinear effects in unpatterned[44,55,56,57,58] or patterned coplanar[54,59,60,61,62,63,64], microstrip[65,66,67] or stripline arrangements[68,69] using Y-123 or Tl-2212. This review does not attempt to be complete but rather to summarize general trends.

As demonstrated in Fig. 6, the field dependence of Z_s provides information on the high-frequency performance of HTS supplementary to that obtained from $Z_s(T)$[70]. The left part of the figure displays $R_s(T)$ at the fundamental mode at 8 GHz (n=1) and at its first harmonic at 16 GHz (n=2) for two different coplanar resonators (samples 646B and 770) patterned from 350 nm thick Y-123 films on MgO substrates. The surface resistance of the two samples differed only by about 10 μΩ over the whole temperature range. In contrast to this similarity, the films exhibited drastically different power performances at 15 K (right-hand part of Fig. 6). Sample 646 B displayed a gradual increase of R_s with B_{rf} already at very small field levels (1 A/m corresponds to $4\pi/10^4$ mT) and a strong increase above 0.25 mT, while R_s of sample 770 remained constant up to about 25 mT. Since the growth conditions were different for the two films, this result was attributed to the presence of defects.

Many authors reported a quadratic increase of R_s with B_{rf} above 0.1 mT with a quartic (or even stronger) dependence becoming dominant at a frequency and temperature dependent field value B_{cr}[65,66,68].

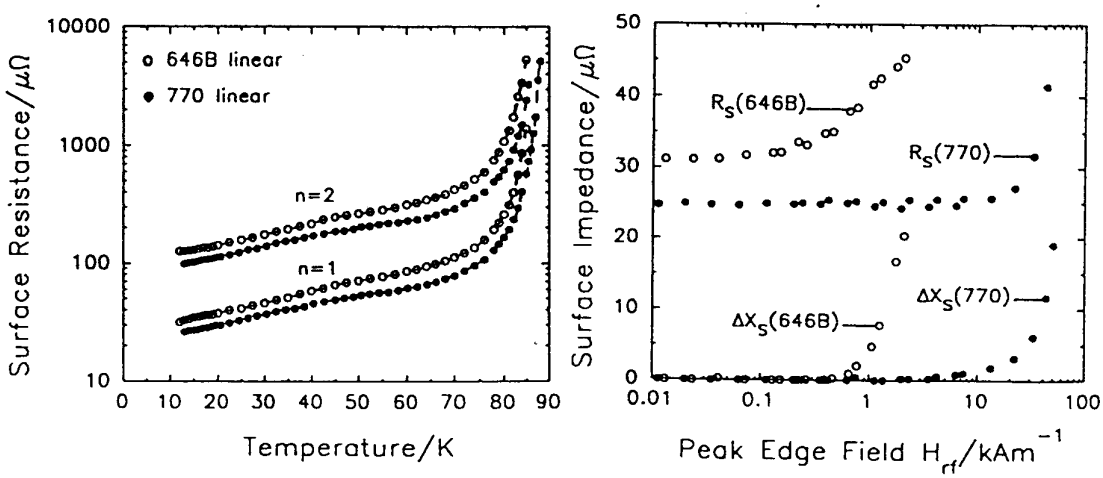

Fig. 6: Left: $R_s(T)$ of two linear coplanar resonators (open and filled symbols, 646B and 770) obtained in the fundamental mode (n=1) at 8 GHz and its first harmonic (n=2)[70]. Right: Dependence of R_s of the same samples on the peak edge field at 15 K.

Tab. 1 summarizes recent data on the maximum reported field levels obtained for different samples at different frequencies and temperatures. The $R_s(B_{rf})$ characteristics are divided into three categories: Type A describes constant R_s at $B_{rf}<B_{cr}$ with a sharp increase of losses at higher fields. Type B represents quadratic $R_s(B_{rf})$, while type C summarizes other power-dependences. Except for the data in rows 11, 12 and 14, which were obtained in pulsed measurements with pulse lengths (intervals) of ≤ ms (about 10 ms), the field dependence of Z_s was deduced from slow (> 30 ms) frequency sweeps across the resonant frequency. The cooling conditions also differed for the listed experiments. The data reveal a large scatter which is related to the many different deposition and measurement techniques applied. Accordingly, the reported B_{cr}-values seem uncorrelated with the film thickness or the surface resistance at low field levels. Also, no general frequency dependence of B_{cr} has been found between 1.5 and 15 GHz[60,71]. Some groups reported correlations between the slope $\partial R_s/\partial B_{rf}$ and the critical current density[55,56,61].

Table 1: Data on the nonlinear surface resistance of Y-123 and Tl-2212 samples.

HTS (substrate)[a]	Film thickness [nm]	Type of device	Frequency [GHz]	Temperature [K]	R_s at small B_{rf} [μΩ]	Crossover field B_{cr}[b] [mT]	Type of $R_s(B_{rf})$[c]	Remarks
Y-123 (MgO)	180-350	coplanar resonator	8	15	20-50	5-25	A	1
Y-123 (LAO)	350	coplanar resonator	5.2, 10.4, 15.6	15	25, 100, 230	9-19	A	2
Y-123 (MgO)	350	coplanar resonator	8	15	25 33	0.7 12.5	A A,C	3
Y-123 (MgO)	800	coplanar resonator	5.7	4.2	≥ 35	0.1-4	A,B	4
Y-123 (LAO)	200	coplanar resonator	6.2	50 50	60 75	3.5 5	B,C B,C	5
Y-123 (LAO)	380	microstrip ring	3.7	70-77	not cited	7.5-10	B	6
Y-123 (LAO)	200-300	meander microstrip	3	7	50-100	2	B	7
Y-123 (LAO)	700	meander stripline	1.5	4.2 77	4.3 15	28 5	B B	8
Y-123 (LAO)	700	meander stripline	1.5	4.2 77	6 20	≥ 50 ≥ 15	B B	9
Y-123 (LAO)	250	microstrip disk	3.6	77	not cited	≤ 3	A	10
Y-123 (MgO)	350	un-patterned	21.5	4.2	100	12	A	11
Y-123 (LAO)	380 560 330	un-patterned	19	77 77 4.2 50 77	≤ 2000 ≤ 2000 200 500 750	7 1.8 ≥ 27 ≥ 23 14	A A A C C	12
Y-123 (LAO)	300	un-patterned	5.6	50	not cited	13	A,C	13
Tl-2212 (LAO)	250	un-patterned	19	4.2 77	≤ 1000 ≤ 1800	1 ≤ 1	C C	14
Tl-2212 (LAO)	700	un-patterned	5.6	4.2 80	18 60	0.5 0.3	A A	15

[a]: LAO denotes $LaAlO_3$. [b]: The values in this column present the threshold fields above which R_s increases strongly in type A behavior. For type B characteristics, the data denote the field level at which quadratic behavior changes into a quartic or stronger dependence. [c]: Type A denotes curves where R_s remains constant up to the field level cited in the preceding column. Type B stands for quadratic $R_s(B_{rf})$ dependences, type C for other behavior than described by types A or B.
Remarks: 1: Data comprize a set of differently prepared films[60]. 2: Data obtained at the fundamental, first and second harmonic mode[60]. 3: Data correspond to differently prepared films[70]. The film with higher $R_s(0)$ showed a slight increase of R_s already above 0.1 mT. 4: The data comprize results of differently prepared films. Type B was reported for the film with the lower B_{cr}[64]. 5: The B_{cr} values are positively correlated to the critical current densities[61] J_c=1.7 and 3.0 MA/cm^2. 6: The characteristic field levels were not cited by the authors but extracted graphically from their $R_s(B_{rf})$ curves[65]. 7: The authors note that the high residual resistance is likely to be caused by the teflon spacer between signal line and ground plate[66]. 8: The characteristic field was reported in Ref. 71 to vary with reduced temperature as $(1-t^2)$[68]. Quadratic behavior was observed above 0.05 mT. 9: The record values were reported in Ref. 74 for magnetron sputtered films. The B_{cr}-values denote the field levels at which R_s has increased significantly from its low-field value. 10: Data from Ref. 56. 11: The data were measured in a Nb host cavity by endplate replacement[55]. 12: The data were measured for films of 1" diameter and different thicknesses in a sapphire resonator[56]. The low-field R_s-value was likely to be affected by parasitic losses. The B_{cr}-values at 4.2 and 50 K were limited by the measurement system. The characteristic field of a 2"-diameter -film was reported[57] to be 5 mT at 77 K. 13: $R_s(B_{rf})$ increased linearly with field at low field levels[58]. 14: The measurement technique is the same as in row 12[72]. R_s increased gradually with B_{rf} from the lowest investigated level (0.01 mT). 15: The data were obtained on 2"-diameter-films using a sapphire resonator[44,73].

Fig. 7 compares the remaining data of Tab. 1 which might be correlated. Interestingly, the maximum field values at 4.2 K were obtained on patterned devices[74]. This fact might reflect the field enhancement in such samples which allows more easily to excite strong fields at the edges of the signal lines compared to unpatterned films. Furthermore, the data do not indicate film damage which could have been induced from the patterning process. A similar conclusion was drawn from a set of measurements performed with one sample before and after patterning[75]. The statistics indicates type A (bright columns in Fig. 7) to occur mostly at low temperatures, except for the (micro)stripline experiments, whereas types B and C (black and grey columns) prevail at elevated temperatures. It is remarkable that none of the maximum field levels significantly exceeded the lower critical field of the investigated HTS. Considering that B_{c1} scales as Φ_0/λ^2 yields $B_{c1}(t)/B_{c1}(0)=1-t^2$ (Sec. 2.2.1). Such a temperature dependence was found experimentally in Ref. 71, and it describes the maximum B_{cr}-values at the different temperatures in Tab. 1 and Fig. 7 reasonably well. The peak current densities corresponding to B_{cr} were reported to be about 10^6 to 10^7 A/cm^2.

Time-resolved measurements of the dynamic nonlinear response of Y-123 films indicated basically two different loss mechanisms (see also Sec. 4.4). The impulse response of thin coplanar transmission lines to picosecond pulses revealed a "slow" effect with a time constant of the order of 10 ns and a nonthermal "fast" effect (< 30 ps)[63]. The slow response was attributed to local heating effects whereas the physical origin of the fast nonlinearity could not be explained. Similar time scales were observed for the photoresponse of thin current-biased HTS films to picosecond laser pulses at wavelengths of 1.06 and 0.80 μm[76,77]. The authors attributed the widths of the photoresponse pulses of about 30 ps to nonequilibrium mechanisms. Due to phonon relaxation processes, the fast signal was followed by a much slower (about 7ns) thermal response. Response times of 100 to 200 nm thick Y-123 films of as low as 1.5 ps were reported recently at 79 K for 150 fs laser pulses at 0.79 μm[78].

Many different loss mechanisms could be responsible for the nonlinear phenomena observed in the frequency-domain measurements. Intrinsic pairbreaking effects[79], Josephson behavior[80,71,81,82], bulk vortex dynamics[83] and combinations of these[11,68,84] as

well as critical state effects[11,65] have been proposed so far. The most often cited approach[68] assumes Josephson behavior to be dominant at low and intermediate field levels $B_{rf} \leq B_{cr}$, whereas at higher field levels bulk vortex dynamics would dictate the nonlinear $R_s(B_{rf})$. This model is undoubtedly powerful in describing many data quantitatively very well. However, the physical meaning of the fit parameters (Josephson critical current densities $>10^6$ A/cm^2, normal junction resistances of only a few mΩ and inherent grain sizes about 3 μm) becomes questionable regarding the irrelevance of granular effects in describing $R_s(T,f)$, and referring to realistic data on artifical HTS grain boundary Josephson junctions[2]. Furthermore, the application of the model is restricted to the type-B characteristics mentioned in Tab. 1, whereas type-A or -C curves were not considered.

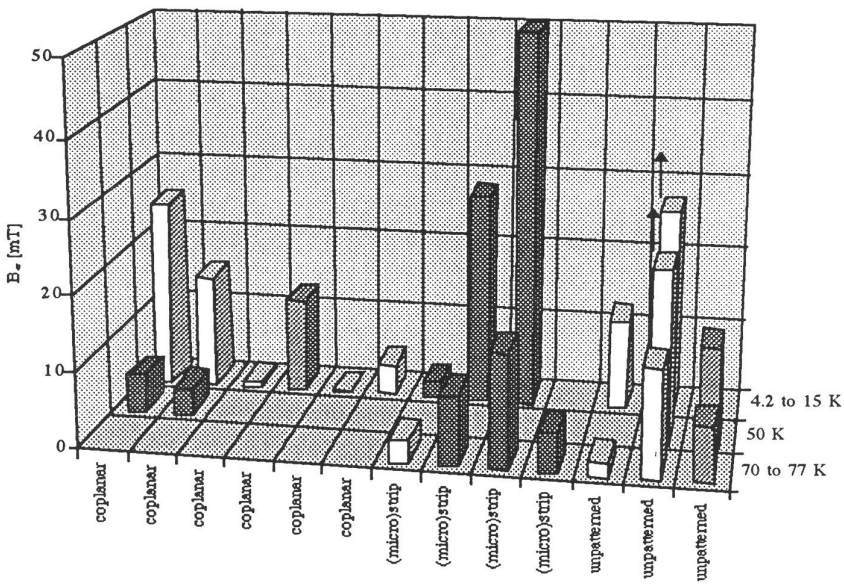

Fig. 7: Statistical view of the data in Tab. 1, sorted after temperatures. Bright and dark columns respresent types A and B as defined in Tab. 1, grey columns indicate type C. The arrows indicate power limitation from the Nb endplate.

The data obtained from frequency and time domain investigations contain supplementary informations about the nature of the nonlinear losses, which have not yet been analyzed in a comprehensive manner. At least, thermal effects must not be neglected in interpreting the nonlinear $R_s(B_{rf})$ since the described experiments applied high-power excitations that were very long compared to the thermal time scale deduced from the time-domain experiments.

Some remarks should be added which might be relevant for a consistent description of $Z_s(B_{rf})$. The main ingredient to the granular model is a microwave current-dependent Josephson inductance[68], $L_J(I_{rf})/L_J(0)=[1-(I_{rf}/I_{cJ})^2]^{-1/2}$. $L_{kin}(t)/L_{kin}(0)=\lambda(t)/\lambda(0)=[1-t^2]^{-1/2}$ is obtained when kinetic effects are considered to result from a thermal suppression of the fraction of paired charge carriers, $x_s(t)=1-t^2$. The temperature t denotes the local temperature of the electronic system (cf. Sec. 4.4.1) rather than the measured value. Assuming, e. g., a linear relationship between microwave current amplitude and this temperature, makes both expressions phenomenologically undistinguishable. Linear I_{rf}-versus-t relations can, in principle, be obtained for certain thermal boundary conditions[85].

Altogether, thermal effects seem essential for an improved modelling of $Z_s(T,B_{rf})$, especially at higher temperature where type B and C characteristics are dominant.

In summary, the power-dependent surface resistance of HTS indicates two different regimes. At field levels below B_{cr}, (localized) granular and/or thermal effects might govern $R_s(B_{rf})$. Optimization of $R_s(B_{rf})$ therefore concerns the optimization of the film quality, but also that of cooling the film and the interfaces film-substrate, substrate-housing and housing-coolant. Above B_{cr}, which might tentatively be identified with B_{c1}, bulk vortex penetration seems to limit the maximum achievable B_{rf} values. This is in contrast to LTS where the nucleation of Abrikosov vortices is too slow for B_{c1} to limit $B_{rf,max}$ at such high frequencies[23]. The main difference between HTS and LTS in this respect is the much smaller coherence length and thus the time required for the nucleation of a vortex. Applications at very high field levels would consequently have to exploit the $(1-t^2)$-dependence of B_{cr}, i. e. profit from a reduced operating temperature. As mentioned in Ref. 54, the very low B_{c1}-value of Tl-2212 films (about 1 mT at 80 K) might be a severe drawback for applications of this material at high field levels. Finally, a comprehensive phenomenological understanding of the microwave properties of HTS seems to require a balanced consideration of heating, scattering effects and granularity.

3 SYSTEM IMPLEMENTATION OF HTS MICROWAVE DEVICES

3.1 General remarks

As discussed in several extended reviews [1,2,86], the material engineering of HTS, based on the knowledge of the temperature, frequency and field dependent surface impedance, must be supplemented by proper device engineering in order to meet realistic system requirements. Fig. 8 is a schematic view of aspects which are of major importance in this context.

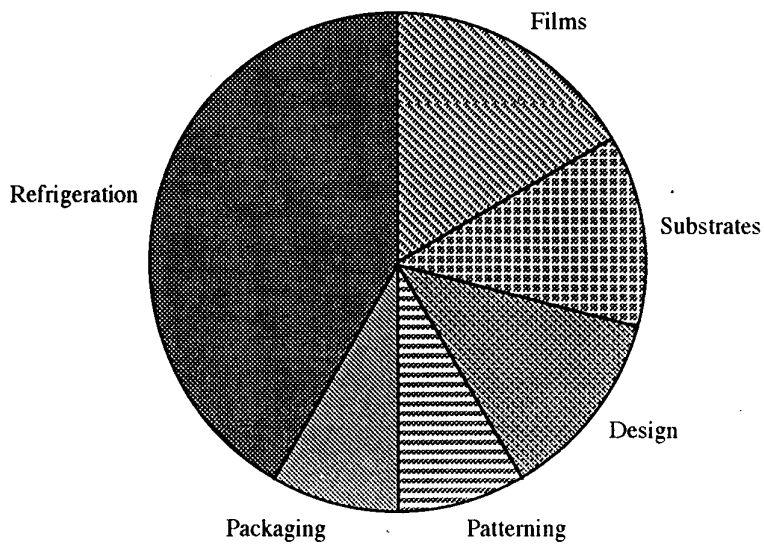

Fig. 8: Schematic representation of aspects which are relevant for system implementation of HTS devices.

The relative weight of the different categories is meant to be qualitative. Since a complete analysis of all aspects is beyond the scope of this contribution, only some

general remarks will be given in the following, which are based on a previous analysis[2]. Reflecting the importance for operational microwave systems, recent developments of refrigeration techniques are treated separately and in greater detail in Sec. 3.2.

Realistic specifications of HTS films comprize, in addition to guaranteeing a reproducible surface impedance (Sec. 2.2), film size, thickness and complexity. Most of the multi-element microwave devices or integrated subsystems, which are presently considered interesting for commercial applications, require areas up to 3" in diameter. Although appropriate deposition techniques have been developed for such film sizes, the density of structural defects like holes or precipitates limits the achievable circuit complexity. Further optimization of the different film preparation techniques should therefore be directed towards reduced defect densities. The film thickness affects the absolute level of surface resistance and reactance if it is of comparable magnitude as the penetration depth. It also determines the maximum power the film can carry before nonlinear effects show up (Sec. 4.1.2). Provided that epitaxial growth can be sustained, film thicknesses of about 700 nm, but at least 300 nm, seem appropriate for most microwave applications of HTS. Double-sided HTS films and multilayer structures are required for the fabrication of many devices, especially if low inductances are involved. Homo- and/or heteropitaxial growth, low interdiffusion and complete oxygenation of all HTS film layers are major requirements for high-quality devices.

It is well recognized that the epitaxial growth of HTS films for microwave applications requires single-crystalline substrates with a suitable permittivity, $Re(\varepsilon)=\varepsilon_r$, low dielectric losses ($\tan\delta=Re(\varepsilon)/Im(\varepsilon)$) and a small mismatch in lattice parameters and thermal expansion. The real part of the complex-valued dielectric constant, ε_r, which should preferrably be isotropic and homogeneous on a microscopic scale, determines the achievable degree of miniaturization and the propagation velocity of guided waves. The temperature dependences of ε_r and $\tan\delta$ should be weak since they might limit the stability of, e. g., high-quality resonators for stable oscillators (Sec. 4.2). The substrates should also be very smooth, with a well defined thickness being constant over the whole size, and chemically inert with respect to the preparation conditions relevant for HTS. The most successfully adopted substrates for Y-123 films are MgO (despite the lattice mismatch), $LaAlO_3$ (LAO) (despite its twinning), $NdGaO_3$ (NGO) and Yttrium-stabilized ZrO_2 (YSZ) (despite their high loss tangents). Regarding the available wafer size and related costs, the low loss tangent and the potential for HTS-semiconductor integration, Al_2O_3, Si and GaAs are also promising candidates if appropriate buffer layers are provided. Tl-2212 films have been deposited successfully onto LAO, NGO and CeO_2-buffered sapphire.

Single microwave circuit elements usually consist of coplanar, microstrip or strip transmission lines, all of which display specific advantages and disadvantages (e. g., single- versus double-sided films, mono- versus multi-layer techniques, characteristic impedance, bandwidth, radiation losses, current-enhancement at edges, sensitivity to substrate properties and so on). The optimum design will depend on the purpose of the device and has to be set individually. For a given type of transmission line, the propagation constant of a strip or a coplanar transmission line can be deduced from numerical simulations taking into account the complex surface impedance of the superconductor. Many commercial computer-aided design codes are known for modeling more complex planar microwave devices like filters. However, the adventure of HTS has uncovered significant weaknesses among which are: The large penetration depth of HTS compared to typical film thicknesses cannot be described by the usually employed thick- or thin-film limits. The large permittivity ($\varepsilon_r>18$) of some substrates adopted for HTS film deposition is not accounted for in many of these computer codes. Finally, some codes for the design of microwave filters cannot handle very small bandwidths ($\leq 1\%$).

The patterning of HTS films into the desired structures also deserves some remarks. Chemical etching usually provides structures with geometrical edge definitions of the order of a few μm. This uncertainty can be dealt with in, e. g., wide transmission lines for operation at low power levels. However, optimized high-power performance, miniaturized circuit elements or highly integrated systems require physical etching processes like Argon ion beam etching through metal masks.

A final and decisive step towards an operational microwave device is an appropriate packaging technique. There are many individual ways to go, and this paragraph summarizes only some of the more important concerns. First, the performance of a microwave circuit can be dramatically altered by the presence of spurious modes in a metallic environment. Proper areal grounding between the groundplate(s) and the housing are essential to prevent parasitic modes between HTS device and metal walls. An appropriate dimensioning of the enclosure is basic for shifting box resonances out of the frequency band of interest. Second, as far as sandwich-type stacked arrangements are employed, airgaps between adjacent substrates alter the performance, reproducibility and stability of the device essentially. Planar interfaces and bonding methods are valuable tools to handle this problem. Third, an efficient means has to be provided to guide the waves from the planar device to the (coaxial) external circuit. Impedance matching, thermal expansion and mechanical manufacturability determine successful solutions. Fourth, the packaging must be mechanically robust enough to withstand the environmental conditions to which a device will be exposed. This is of special concern for possible applications of HTS microwave systems in satellite systems. Fifth, to operate a superconductive system, low operating temperatures have to be provided, sustained and controlled. "Efficient" cooling means to provide conditions for reliable physical operation, to keep costs, weight and maintenance intervals at an economically tolerable level and to pass the threshold related to the public acceptance of superconductive technology.

3.2 Refrigeration

3.2.1 General Requirements All possible processes to provide cooling rely on the first and second principles of thermodynamics. One of the most important consequences of these fundamentals is that the ultimate efficiency of a cyclic process is always limited by the "Carnot" efficiency of a reversible cycle, η_C:

$$\eta_C = \frac{T}{T_{hot} - T} \tag{9}$$

where T_{hot} is the temperature at the warm side of the cooling system. For low temperatures $T \ll T_{hot}$, Eq. (9) yields an efficiency which increases linearly with temperature. For the two boiling points of nitrogen (77 K) and helium (4.2 K) at normal pressure (10^5 Pa) and T_{hot}=300 K, one obtains η_C=0.35 and 0.015. Besides cooling by dissipating the latent heat of liquefied gases, refrigeration can be obtained by expanding working gases (or gas mixtures) at constant entropy or constant enthalpy, the latter being known as the Joule-Thomson process[87]. The efficiency of gas expansion machines is basically improved by employing heat exchangers which are either recuperative (which exploit the backflow of cold gas towards the warm stage of the refrigerator) or regenerative (which rely on the large heat capacity of suitable materials). Powerful refrigeration systems contain a combination of both types and usually consist of multi-stage arrangements. More detailed informations on the physics of refrigerators can be found, e. g., in Ref. 88.

As mentioned in the previous Sec., there will hardly be any commercial application of HTS systems if there is no appropriate cooling system. The meaning of "appropriate" depends on the field of application. For HTS microwave systems, the basic concerns were summarized in Refs. 89,90 (in a sequence which was not meant to reflect the importance of each statement).

1. The desired temperature of operation is one of the major input parameters. The cooling efficiency increases and the required electrical input power, the size and the weight of the cryocooler decrease with increasing operating temperature[91]. On the other hand, the absolute levels of surface resistance, penetration depth and critical current density, the current-carrying capability, the temperature variation of these parameters and the thermal noise improve with decreasing temperature. The resulting temperature range for the application of HTS in microwave devices is therefore expected to be in the range 50 to 80 K and, for high-performance applications, eventually even lower (Fig. 9).

2. The net cooling power required for a stable and reliable operation of a device needs to be known. Its value depends on the complexity of the system (single component versus multi-element system), its internal power consumption (e. g., low-power operation in receivers versus high-power in transmitters), the external heat losses due to thermal and electric leads, and the total thermal capacitance to be cooled, which is determined by the masses and the thermal capacities of the materials used. A tentative interval of 100 mW to 10 W has been assumed in Fig. 9.

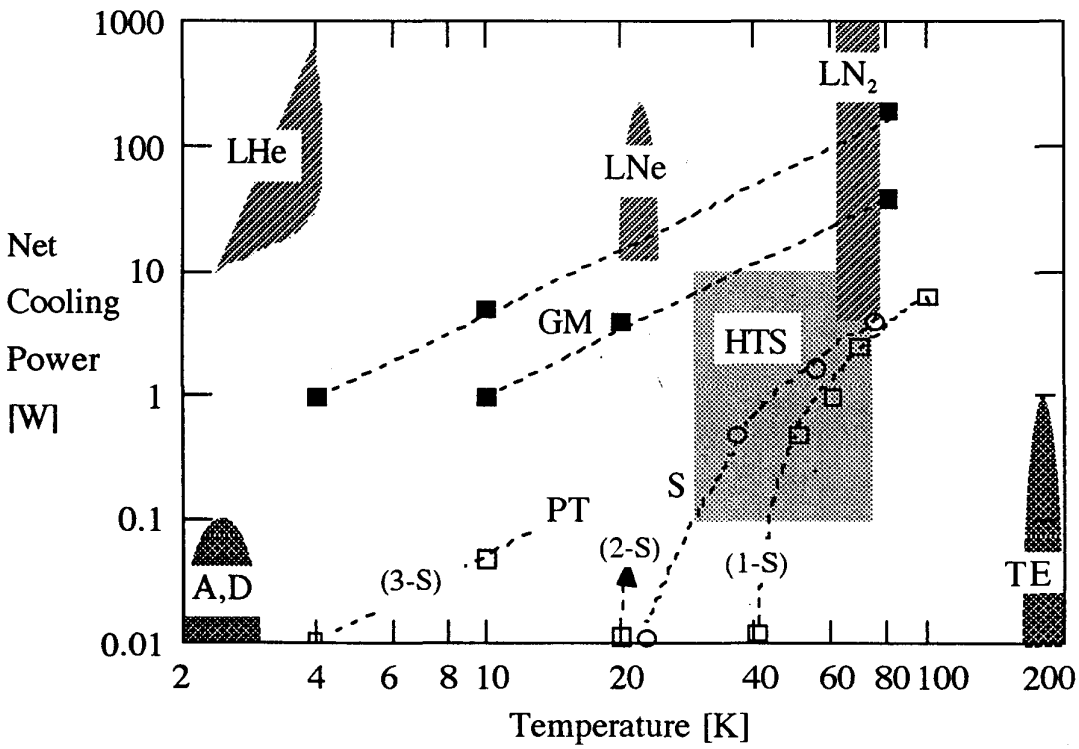

Fig. 9: Net cooling power versus temperature for different cooling mechanisms. Grey dashed areas denote the regimes accessible with the liquid coolants LHe, LNe, and LN_2. The grey rectangle represents the expected regime for microwave applications of HTS. A and D stand for adiabatic demagnetization and dilution refrigeration, GM for Gifford-McMahon, S for Stirling, PT for pulse tube, 1-S, 2-S and 3-S for single, double and triple stages, and TE for thermoelectric. Typical performance obtained with GM-coolers is indicated by filled squares, with S-coolers by circles and with PT-coolers by open squares. The data were deduced from several publications[89,90,91,94].

3. The total electrical input power relative to the net cooling power, sometimes called the "coefficient of performance", determines the choice and possible limitations of the refrigerator. Considering efficiencies of 0.01 η_C, the power needs range between 1.4 kW per Watt at 20 K and 0.3 kW per Watt at 80 K[88].

4. Weight and volume play major roles for the application of HTS microwave devices in satellite-based systems[3]. Typical values for commercial systems are 200, 40, 15 and 1.5 kg per Watt cooling power at 4.2, 10, 20 and 80 K, respectively[91]. The benefit of miniaturized and/or high-performance HTS circuits must not be compensated by bulky or heavy refrigerators. Such a counterbalance would likely prevent HTS from becoming applicable in this field.

5. The cooldown time is another important criterion for a real device. It depends on the device architecture and the packaging as well as on the net cooling power available at the operating temperature. Realistic values are epexted to be around some 10 minutes.

6. Reliability is a major problem of all categories of refrigerators. Liquid coolants handle extreme cooling situations but require expensive and logistically complicated maintenance and refilling (Sec. 3.2.2). Closed-cycle cryocoolers were, until recently, only developed for two extreme cases: either for military purposes (environmental surveillance) or satellite-based systems (military and civilian). While in the former case relatively cheap (about 10^3 US$) systems with a low "mean-time before failure" (MTBF) of a few 10^3 hours became available, refrigerators for the latter purpose were extremely reliable (MTBF$\approx 10^5$ h) but also extremely expensive (about 10^5 US$). The present challenge is therefore to develop reliable (MTBF$\geq 10^4$ h) as well as cheap ($\leq 10^3$ US$) cryocoolers. From recent research successes, this task seems likely to be fulfilled in the near future.

7. The different types of cryocoolers differ strongly in sources of noise and fluctuations of the operating parameters. Stable and precise temperature control, low-level mechanical vibrations and low electromagnetic interferences are vital for applications of HTS to sensitive devices like SQUIDs and bolometric detectors. Novel arrangements of cold heads and sample positioning have been developed to minimize the noise by mechanical, spatial, temporal and electronic noise compensation[92,93].

Along with these numerous criteria, there are many different solutions possible. Furthermore, the rapid progress of HTS technology has enormously been pushing the development of reliable miniaturized coolers[94].

3.2.2 Liquid coolants Liquefied gases like liquid nitrogen (LN_2) have not been considered serious candidates for the refrigeration of HTS microwave systems because of the complex and, more or less, frequent maintenance required. However, they display some remarkable features which might be relevant for a few specific applifications of HTS devices. Liquid coolants allow for immersion or vapor cooling, and numerous revolutionary architectures of bath or gas flow cryostats have been developed since the pioneering work of H. K. Onnes. Only a limited temperature range is accessible in bath cryostats which is determined by the thermodynamic phase diagrams of the gases (marked in Fig. 9 by grey dashed areas).

One advantage of immersion cooling is that very large cooling capacities can be provided for very large areas. For instance, large-scale particle accelerators employing LTS cavities and magnets have been designed with cryostats having volumes of several 10^6 cm^3 and a refrigeration power of tens of kW at an efficiency of up to 0.2 η_C even at T=2 K[95,96]. A high reliablity of MTBF=$5\cdot 10^4$ h was reported which was usually limited by the helium compressor.

On the other extreme, gas flow cryostats have been constructed for high-precision measurements like biomagnetic signal recording[97]. The volume of miniature portable cryostats ranges between 10^2 and 10^3 cm^3. The cryostats are completely made of non-magnetic fiberglass materials with very low residual magnetic noise allowing for an operation in unshielded environment at a level of 20 to 40 $fT/(Hz)^{1/2}$. The temperature can be stabilized within a few mK, and the low helium evaporation enables continuous operation over some 10 to 100 h. Cryostats allowing for upright and reverse positions have been built as well as systems with separations of only a few mm between the cold sample and ambient temperature. Similar dewar systems have been constructed for use of liquid nitrogen (LN_2)[97,98]. Due to the higher temperature, cold-warm distances below 1 mm were achieved. Since the latent heat of LN_2 is a factor of 40 higher than that of LHe, the need for refilling is expected to be correspondingly less frequent.

3.2.3 Closed-cycle cryocoolers Unless bulky systems need to be cooled or extremely stable and quiet operating conditions are required, the use of closed-cycle cryocoolers (CCC) is favoured. The most prominent types are based on the Gifford-McMahon and the Stirling thermodynamic cycles[87,88] (GM and S in Fig. 9). A certain volume of gas, e. g., some liters of helium, is iteratively transferred between a compressing and an expanding stage with intermediate regenerative stages. A phase shift between the mass flow and the pressure cycle provides the cooling effect[99]. The compressing stage in GM-refrigerators is placed outside the cold stage in contrast to the S-type CCC. As a result, GM-systems produce less vibrations, are less sensitive to gas contamination and have a higher reliability (MTBF$\geq 4 \cdot 10^4$ h) compared to S-systems (MTBF$\geq 5 \cdot 10^3$ h)[89]. Commercially available GM-coolers provide typically 1 to 5 W refrigeration power at 10 K, but can hardly be miniaturized[91,94]. Recent progress in the development of CCC resulted in cooling capacities of about 1 W at 4.2 K with efficiencies of 0.01-0.03 η_C using a two-stage GM cooler in combination with rare earth regenerators, a three-stage GM cooler in combination with a Joule-Thomson expansion stage or a three-stage GM cooler exploiting a novel thermodynamic cycle ("Boreas" cycle)[100].

In contrast to the GM-machines, Stirling cryocoolers are suited for applications where small and lightweight systems and small cooling capacities are required. Fig. 10 presents a schematic view of a Stirling refrigerator. The displacer located at the cold stage provides the required phase shift between mass flow and pressure wave[99]. For a 90^0 phase shift between the volume variation at the cold end and the compressor cycle (performing the mechanical work W), most of the gas is compressed at the hot end and expanded at the cold end. As a result, the heat Q is absorbed at the cold head, and an amount Q_0 is produced at the hot stage. The cold moving displacer usually limits the maximum achievable lifetime of such systems, but improvements have been reported recently on the clearance seal technology, the use of linear instead of rotary drive motors and the handling of gas contamination[89,91]. However, the displacer motion causes mechanical vibrations and magnetic interference which can not be tolerated for certain application of highly sensitive detectors[93].

A very promising modification of the Stirling cooler is the pulse tube cooler (PT in Fig. 9, schematic in Fig. 10), in which the moving displacer is eliminated from the expander. It thus has no moving parts in the cold stage and bears a great potential for high reliability and also for miniaturization. The concept of the pulse tube refrigerator is known since 1963[101], but the minimum achieved temperature of a single-stage system so far was only about 120 K. Much better performance has been obtained by modifications of the pulse tube, namely the orifice pulse tube[102] and the double-inlet pulse tube[103], which reached in a single-stage minimum temperatures of 49 and 28 K as summarized in Ref.

104. The required thermodynamic phase shift is obtained by mass flow through an orifice to a reservoir[99]. PT coolers are presently under intense development with respect to an improved understanding of the underlying thermodynamics, different drive types, combination of multiple stages for higher refrigeration power, miniaturization and noise cancellation. Recent data on achieved cooling capacities for single (1-S), double (2-S) and triple (3-S) stage systems are implemented in Fig. 9. It is worth mentioning that the lowest achieved temperature of a 3-stage PT cooler is at present 3.6 K[105]. Very recently, a minimum temperature of 9 K was achieved with a single-stage PT cooler, the warm head of which was cooled by LN_2 to 77 K[106].

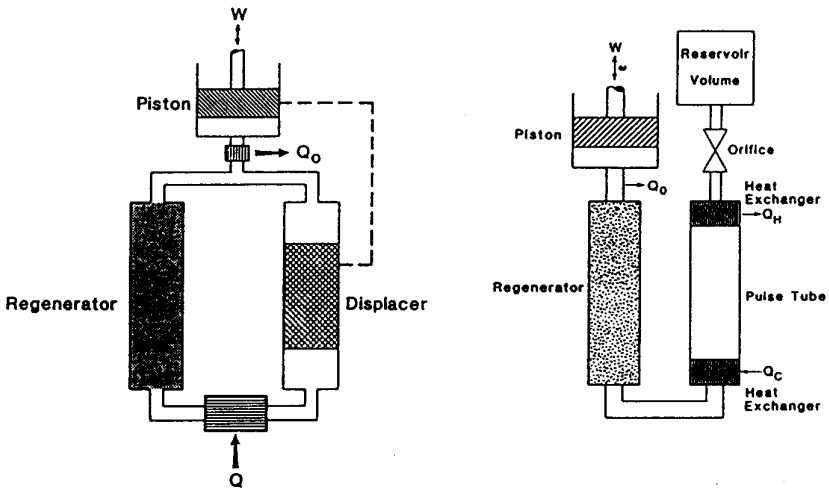

Fig. 10: Schematics of a Stirling (left) and an orifice pulse tube refrigerator (right) with indicated thermodynamic parameters like mechanical work W done at a frequency ω and heats Q_0, Q, Q_H and Q_C produced or absorbed at the different stages[99].

Not many efforts have yet been reported for a complete cryogenic integration of HTS circuits[90]. An important technology push in this respect came from the two phases of the "High-Temperature Superconductivity Space Experiment", HTSSE, conducted by the Naval Research Laboratory in Washington, D.C. (Refs. 107,108 and Sec. 5.1.1). The final system package including about 10 HTS microwave subsystems (contributing a mass of about 3 kg), cold bus, ambient temperature frame, cryocooler and related electronics and multi-layer insulation weighed about 30 kg. Under optimized thermal packaging, the total heat load amounted to 350 mW at about 80 K.

In summary, GM-, S- and PT refrigerators provide sufficient refrigeration power for cooling HTS microwave systems (Fig. 9). Improved reliability, miniature designs and reasonable noise performance have already been demonstrated. However, further optimization of these issues as well as the need for low costs remain to be pursued. Comparing the present state-of-the-art in CCC technology with that three years ago, enormous developments have been achieved, and future reviews of this field might likely report further important breakthroughs in the cryogenic engineering of superconductors.

4 PASSIVE HTS MICROWAVE COMPONENTS

4.1 General considerations

4.1.1 Linear transmission line elements The microwave response of a linear two-port is completely described by the scattering parameters $S_{ij}=|S_{ij}|\cdot\exp\{-i\Phi_{ij}\}$ with i,j=1,2. For

example, S_{11} describes the amplitude of the voltage reflected at port 1, normalized to the amplitude of the incident voltage. In case of a reciprocal device, the coefficients of voltage transmission from port 2 to 1 and vice versa, S_{12} and S_{21}, are identical. Any such a device can be characterized by the frequency dependence of the dissipative response (insertion loss $a_{IL}=-20\cdot\log|S_{21}|$) and by that of the dispersive response (group delay $\tau_{gr}=d\Phi_{21}/d\omega$). If the device can be assumed lossless, energy conservation requires that $|S_{11}|^2=|S_{22}|^2=1-|S_{21}|^2$ and $2\Phi_{21}=\Phi_{11}+\Phi_{22}\pm\pi$. The stored energy W, averaged over a cycle $2\pi/\omega$ and normalized to the incident power, can be expressed as the "storage quality factor" Q_{store}:

$$Q_{store}=\frac{\omega W}{P_{diss}}=\omega\cdot\{(1-|S_{21}|^2)\frac{d\Phi_{11}}{d\omega}+|S_{21}|^2\frac{d\Phi_{21}}{d\omega}\} \tag{10}$$

Eq. (10) holds if port 2 is terminated by a matched load. The scattering parameters and the phase response can be related, in case of a resonant system, to the loaded quality factor of the resonator, Q_L:

$$|S_{ii}|=1-\frac{2Q_L}{Q_{coupl\,i}}\quad\text{and}\quad|S_{ij}|=\frac{2Q_L}{(Q_{coupl\,i}\cdot Q_{coupl\,j})^{1/2}}$$

$$\tan(\Phi_{ij})=\frac{1}{Q_L}\frac{\omega^2}{\omega_0^2-\omega^2}\quad\text{and}\quad\tau_{gr}=\frac{2Q_L}{\omega} \tag{11}$$

where $Q_{coupl,i}$ describes the stored energy normalized to the energy per cycle coupled through port i. Considering all possible loss mechanisms, conservation of energy translates into a sum rule for inverse Q-values:

$$\frac{1}{Q_L}=\frac{1}{Q_{diss}}+\frac{1}{Q_{coupl}}+\frac{1}{Q_{rad}} \tag{12}$$

where the dissipative term comprizes losses in the conductors as well as in the dielectric (cf. Eq. (13)). Except for pulsed measurements with a pulse shorter than $(2\pi\Delta f_{1/2})^{-1}$, where $\Delta f_{1/2}$ is the 3-dB bandwidth of the transmitted power, Q_{coupl} can be identified with Q_{store}. The dissipation term in Eq. (12) is determined by the surface resistance of the conductors and the loss tangent of the dielectrics:

$$\frac{1}{Q_{diss}}=\frac{1}{Q_{cond}}+\frac{1}{Q_{diel}}=\gamma_{cond}\frac{R_s}{Z_0}+\gamma_{diel}\tan\delta \tag{13}$$

with γ_i weighting the contribution of each loss mechanism to the total dissipation and $Z_0=120\pi$ (in units of Ω) the free-space wave-impedance.

This analysis can be applied to many different kinds of devices, including single as well as multiple circuit elements. The microwave response of, e. g., a single bandpass filter can be described by low in-band insertion loss, high out-of-band rejection and steep skirts in a prescribed passband. The value of $|S_{21}|$ at the center frequency and the steepnees of the phase response are determined, according to Eq. (11), by the loaded quality factor. With properly chosen substrate materials, geometric arrangements minimizing radiative losses and for weak coupling, Q_L is limited by Q_{cond} and thus by R_s (Eqs. (12) and (13)). For a bandpass filter at center frequency f_0 and bandwidth Δf, which consists of N coupled filter elements, the stored energy is given by

$$Q_{store}=\omega\tau_{Gr}\geq\frac{f_0}{\Delta f}\sum_{k=1}^{N}\gamma_k \tag{14}$$

with γ_k the weights of the single filter elements. Steep filter skirts (i. e. small Δf) require high Q_{store}-values which result in an enhanced sensitivity of the device to power dissipation in the conductor (Eq. (12)). As another example, an allpass filter is characterized by low insertion loss at all frequencies and a group delay with specified frequency dependence. Special cases are nondispersive delay lines with τ_{gr}=constant and chirp filters with a linear group delay $\tau_{gr} \propto \omega$. The resulting group delay of a chain of allpass sections is simply given by the sum of the individual group delays of each element. Possible applications concern, e. g., group-delay equalizers and chirp-filters with large products of differential delay time and bandwidth. The desire for large group delays implies again a high sensitivity of such devices to the surface resistance. Finally, single antenna elements or antenna arrays can be considered as special types of resonators with a dominant role of the radiative term Q_{rad} in Eq. (12) (Sec. 4.3).

4.1.2 Power handling capability Another very important issue is the performance of a HTS device at elevated power levels (Sec. 2.2.3). The maximum surface current $H_{s,max}$ in a resonant two-port is related to the stored energy and to the incident power by

$$H_{s,max} = \gamma_{pow}(\omega W)^{1/2} = \gamma_{pow} Q_L \left(\frac{P_{inc}}{Q_{coupl1}}\right)^{1/2} \qquad (15)$$

The coefficient γ_{pow} (in units A/m/W$^{1/2}$) describes the transformation of power fed to the circuit via port 1 into the maximum field amplitude which eventually limits the device performance. This coefficient can be related to the dissipative weight γ_{cond} in Eq. (13) by

$$\gamma_{pow}^2 = \frac{2\gamma_{cond}}{Z_0 A} \cdot \frac{\max\{H_s^2\}_A}{\mathrm{ave}\{H_s^2\}_A} \qquad (16)$$

where A is the surface contributing to R_s and $\max\{H_s^2\}_A$ (or $\mathrm{ave}\{H_s^2\}_A$) is the maximum (or average) of H_s^2 over this area. Similar equations can be set up for the maximum amplitude of the total current I_{rf} or of the corresponding flux density B_{rf}. It can be concluded from Eqs. (15) and (16) that large values of $H_{s,max}$ on the HTS surface occur in high-Q and/or in low-dimensional (small A) devices or in devices where R_s contributes much to the total losses (large γ_{cond}). Microwave components with high power capability should accordingly be fabricated with dielectric-loaded resonators (Sec. 4.2.3) or parallel-plate resonators rather than with stripline, coplanar or lumped-element devices[1].

In summary, the application of HTS to linear passive microwave devices is especially challenging if a high storage factor is required (e. g., in highly dispersive components), if the power dissipation in the conductor limits the achievable insertion loss (e. g. in high-Q devices or lumped-element circuits) and if a high degree of linearity (e. g. in receiver front ends) or large circulating powers (e. g. in transmitters) are required.

4.2 Nonradiating devices

4.2.1 Planar HTS transmission lines Nonresonant transmission lines are building elements of integrated microwave devices. They can be designed as coplanar, microstrip or stripline configurations[2]. If pulse propagation is considered, e. g. in transmission lines for optical communication systems[109] or in pulsed digital circuits[110], large bandwidths are required which determine the circuit design.

Resonant transmission lines are key elements for planar filters. Furthermore, they are valuable tools for measuring the propagation constant and the power-handling capability of HTS. The simplest way to obtain resonant structures is to terminate

transmission lines electrically or magnetically such that the resulting lengths are multiples of a quarter or half of the guided wavelength. Coplanar structures benefit from the single-sided conductor structure but display, for a given quality of the conductor material and a given wave impedance, a considerably higher attenuation compared to microstrip lines[111]. The lower insertion loss of microstrip lines is achieved at the expense of double-sided conductor arrangements. In order to build highly integrated circuits with a given wave impedance, both the width of the stripline and the thickness of the substrate have to be reduced. Since the latter cannot be arbitrarily decreased, multilayer structures with heteroepitaxial layers of HTS and dielectric films are required.

4.2.2 Planar HTS transmission line filters and delay lines Filters are key elements in analog signal processing like channelizing the input signals of a receiving unit (multiplexing) or combining different channels at the transmitting stage (demultiplexing). Of basic concern are well-defined (and adjustable) center frequencies, small bandwidths, steep skirts, prescribed values of in-band insertion loss and out-of-band rejection, high linearity and, eventually, poles at specified frequencies. According to Eq. (14), high-order (N>6, $\Sigma\gamma_k$>10) bandpass filters with narrow relative bandwidths of $\Delta f/f_0 \leq 1\%$ yield a storage factor $Q_{store}>10^3$. For the insertion loss at center frequency to be below 0.5 dB, an unloaded quality factor of typically $Q_{diss}=10^4$ and a high power-carrying capability are therefore required. At frequencies below 15 GHz, such values can in principle be achieved with normalconducting waveguide structures, but a compact planar design requires the use of superconducting components. Single microstrip and stripline resonators with Q values of $6\cdot10^4$ at 1.5 to 2 GHz, $5.4\cdot10^4$ at 3.6 GHz, $4.5\cdot10^4$ at 4.4 GHz and $1.5\cdot10^4$ at 6.9 GHz were reported at 70 to 77 K by several groups[56,109,112,113,114]. Such Q-values suffice for implementation in input multiplexers and/or output multiplexers of mobile communication systems provided that the required linear power performance be achieved, and that tunable filters with specified frequency responses be constructed.

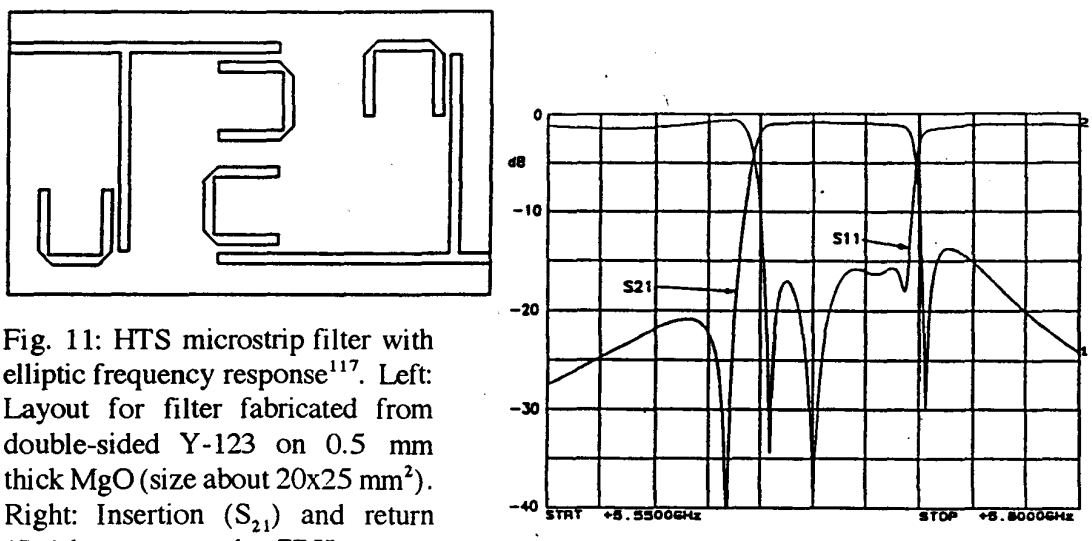

Fig. 11: HTS microstrip filter with elliptic frequency response[117]. Left: Layout for filter fabricated from double-sided Y-123 on 0.5 mm thick MgO (size about 20x25 mm^2). Right: Insertion (S_{21}) and return (S_{11}) loss measured at 77 K.

Most of the planar Y-123 and Tl-2212 or 2223 filters demonstrated so far employ parallel-coupled transmission line resonators[1,72,86,115,116]. The impact of the filter design on planar HTS transmission line filters at low frequencies (≤2 GHz) and on the resulting power-handling capability were analyzed in Ref. 115. Parallel-coupled filters with only adjacent resonators contributing to the filter characteristic result in frequency responses (e.

g., Chebyshev response with uniform ripples in the passband) where the attenuation poles are located at infinite frequency. In contrast, an elliptic filter exhibits attenuation poles at finite frequencies, which can be close to the transition frequencies of the passband. Such filters allow for much steeper skirts for a given order N of single elements. However, elliptic filters require a more sophisticated design since proper coupling needs to be assured not only between adjacent elements. Fig. 11 presents the layout and experimental results obtained with a four-stage extracted pole elliptic filter fabricated from a Y-123 film on MgO at 77 K[117]. The 3-dB bandwidth of the filter was 1.3% and the insertion loss at center frequency 0.61 dB. Planar allpass and bandpass filters can also be constructed with reflection-type approaches[111]. Results on bandpass and chirp filters have been demonstrated for HTS microstrip and coplanar line segments[118,119].

Aiming at high-power filters, several possible approaches have been identified[115,120]. These include: 1. the reduction of current nonuniformity across the filter cross-section by proper design, 2. the increase of the width of the filter segments in order to release the ratio of current-density to total current, 3. the reduction of the coefficient γ_{pow} (Sec. 4.1.2) by proper design or the use of higher-order modes, 4. the increase of the film thickness to reduce the edge enhancement of the current.

Fig. 12 presents the layout and experimental results on a five-pole forward-coupled microstrip filter with 1% fractional bandwidth at 2 GHz on a double sided 2" LAO wafer[120]. The design was optimized for high power-handling capability along with the steps 1, 2 and 4. At 58 K, a power-induced degradation of the filter performance was observed at a transmission level of 40 dBm (or 10 W), while 36 W (45 dBm) could be handled at 45 K in the best sample with a maximum band-edge compression of 0.15 dB[115]. Similar approaches were reported for disk-shaped microstrip filters[69,121,122] providing a linear filter performance up to about 15 W at different temperatures.

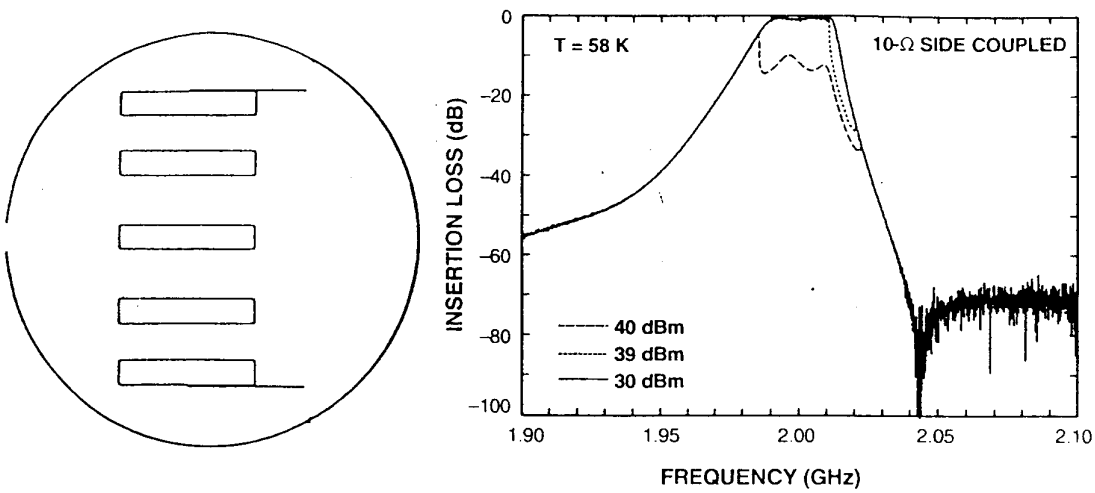

Fig. 12: Mask layout of a forward-coupled filter at 2 GHz (left) and plot of insertion loss versus frequency for different input power levels at 58 K (right)[120].

Delay lines can be considered another special type of transmission line exhibiting a low and generally frequency-independent insertion loss but frequency-dependent group delays. Depending on the final application, small- and large bandwidth delay lines can be of interest. The product of group delay times bandwidth, TB, parametrizes the number of information cycles gathered coherently in the filter. As reviewed in Ref. 1, the large TB-values achievable with superconducting circuits brought about delay lines for pulse compressing, convolving and spectrum analyzing over bandwidths from 2 to 100 GHz.

TB-values up to 100 were reported for nondispersive HTS delay lines on single 2" LAO wafers between 3 and 9 GHz[1,119,123]. Dispersive delay lines for chirp-filters were recently reported with TB≥24 ns·2 GHz and a maximum delay up to 40 ns on thinned 2" LAO substrates[124]. Circuit demonstrations covered instantaneous frequency meters[125,126] and compressive receivers[127]. Small-bandwidth delay lines are of interest for group-delay equalizers in communication systems where the signals are confined to narrow frequency bands. Referring to Eq.(11), large group delays $\tau_{gr}=2Q_L/\omega$ can be obtained with high-Q resonators (e. g., 530 ns for $Q_L=10^4$ and $f_0=3$ GHz), though at the expense of a small TB product of $TB=\tau_{gr}\cdot\Delta f_{1/2}=1/\pi$.

4.2.3 Dielectric resonators Very high unloaded Q-values and high power handling capability are required for, e. g., low-phase noise oscillators in radar and satellite communication systems. As discussed in Sec. 4.1, such performance criteria can best be achieved with three-dimensional resonators. In order to reduce the volume as much as possible and to benefit simultaneously from operation temperatures accessible with compact cryocoolers (Fig. 9), dielectric-loaded resonators (DRs) shielded with HTS films were reported[56,58,86,128,129,130,131,132,133]. The concept of DRs is well known[134]. A typical experimental setup of a DR is shown in Fig. 13. The Q-values achieved with HTS-DRs at different frequencies and for different dielectrics are summarized in Tab. 2.

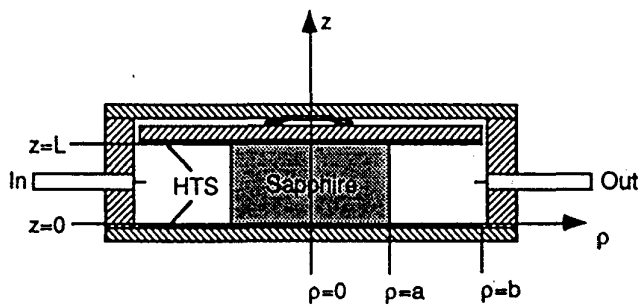

Fig. 13: Typical setup for a dielectric-loaded HTS resonator[130].

In order to evaluate the data listed in the table, the loss contributions $1/Q_{cond}$ and $1/Q_{diel}$ from Eqs. (12) and (13), or γ_{cond}, γ_{diel} and tanδ need to be considered. All data were measured in the TE_{011} mode which provides the optimum field distribution with respect to vanishing electric fields at the circumference of the dielectric rods and low field amplitudes at the endplates. The resonant frequency of this mode can be approximated for a given value of D_{diel}/H_{diel} by[134]

$$f_0(TE_{011}) \approx \frac{c}{2\pi D_{diel}\varepsilon_r^{1/2}}\{4x_{01}^2+(\pi\frac{D_{diel}}{H_{diel}})^2\}^{1/2} \qquad (17)$$

with $x_{01}\approx 3.8317$ the first zero of the first Bessel function. Eq. (17) describes the scaling of f_0 with D_{diel} and ε_r correctly but overestimates the exact resonant frequencies[135] by about 10%. In order to reduce field leakage from the dielectric, large D_{diel}/H_{diel} are desirable. This leads, at a given frequency, to a trade-off between field confinement and resonator volume. As indicated in Tab. 2, $D_{diel}/H_{diel}=2$ was chosen in most experiments. The dissipation factor γ_{cond} can then be expressed as[2]

$$\gamma_{cond}=\frac{4\pi^2}{(\pi^2+x_{01}^2)^{3/2}}\cdot\frac{\{1+\varepsilon_r(1-\gamma_{diel})\}}{(2-\gamma_{diel})}\cdot\varepsilon_r^{1/2} \qquad (18)$$

The volume of a DR varies as $D_{diel}^2 \cdot H_{diel}$. At given frequency, the diameter (volume) of the dielectric thus scales as $\varepsilon_r^{-1/2}$ (ε_r^{-1}), and, according to Eq. (16), the field calibration factor γ_{pow} as $\varepsilon_r^{3/2}$. In order to obtain high Q-values at minimum volume and high power-handling capability, dielectrics with large permittivity and low loss tangent are favorable.

Tab. 2: Survey of dielectric-loaded HTS resonators with different dielectrics.

f_0 [GHz]	Dielectric material	D_{diel} [mm]	D_{diel}/H_{diel}	D_{HTS} [mm]	$10^{-6} \cdot Q_0$ (high T)	$10^{-6} \cdot Q_0$ (low T)	γ_{cond}	$1-\gamma_{diel}$	Re-mark
5.55	sapphire	25.4	2.12	50.8	3.0	9.0	1.812	0.02	1
5.6	LAO	15.2	1.77	30x30	0.4	0.8	2.600	0.02	2
9.7	Rutile	4.0	2.00	8.0	0.6	0.1	5.386	---	3
11.62	LAO	7.1	1.73	20x20	0.1	0.4	2.356	0.008	4
18.38	LAO	3.1	0.78	11	---	0.5	---	0.033	5
19.5	sapphire	7.0	2.00	≥ 25.4	0.6	2.0	1.661	---	6
27.45	sapphire	5.0	2.00	12x12	0.2	0.9	1.661	---	7

Remarks: f_0 denotes the resonant frequency, D_{diel} and H_{diel} the diameter and the height of the dielectric rods, D_{HTS} the diameter or the lengths and widths of the HTS samples, and Q_0 at low (high) T the unloaded Q-factors at temperatures between 70 and 80 K (4.2 and 20 K).

1: The data were obtained with high-purity sapphires and using Tl-2212 films[130]. 2: The data were measured with a $LaAlO_3$ rod[58] with ε_r=23.4 and tanδ ≤5·10^{-6}. 3: The dielectric was a high-purity rutile (TiO_2)[132] with ε_r=85-105 and tanδ ≤5·10^{-6}. 4: Same as for 2[131]. 5: The data are part of an extended analysis of the dielectric properties of different materials[128]. The resonators were not designed for ultimate Q-values but for maximum sensitivity to tanδ. The HTS films were Tl-compounds. 6: The data were measured with one HTS sample and one Niobium shield. The γ_{cond}-value of the HTS film is half of the value given in the table[56]. 7: Same as for 1[133].

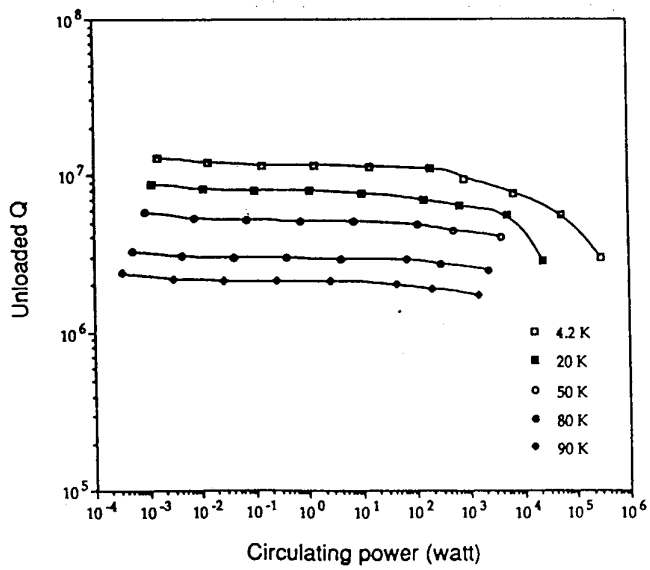

Fig. 14: Power-handling capability as obtained with a sapphire resonator at 5.6 GHz using two 2" Tl-2212 films[130].

The data in Tab. 2 demonstrate the possibility of achieving unloaded Q-values of the order of 10^6, even at elevated temperatures and for such different materials as $LaAlO_3$, sapphire and rutile. It is complicated, however, to compare the Q_0-data for the different frequencies and dielectrics since the frequency scaling depends on the relative contributions of R_s and tanδ, which differed for the experiments. R_s can roughly be scaled as f^2 (Sec. 2.2.2). The frequency and temperature dependences of the loss tangent of pure dielectrics were calculated[136] for centrosymmetric samples as $f^n T^{6-n}$. The measured

temperature and frequency dependences of tanδ, however, deviated from expectation and were found to depend strongly on purity and microstructure of the material[2]. For a given frequency and temperature, the optimum design of a DR will be determined by a clever counterbalance between R_s and tanδ.

Fig. 14 shows results on the power handling capability of a DR in terms of the circulating power[2] $P_{circ}=1/2\omega W$ measured with Tl-2212 films at 5.6 GHz[130]. The achieved performance is very promising for realisitc applications in miniature HTS low-phase noise oscillators[1, 86,129]. Furthermore, miniaturized multipole filter structures based on HTS DRs have been reported[137]. The remaining challenges concern the development of reliable tuning elements and further optimization with respect to suppressed leakage fields, reduced microphonics and improved temperature stability.

4.2.4 Planar lumped-element HTS filters In contrast to planar filter structures composed of distributed circuit elements, where the geometric dimension of the single resonators is determined by the guided wavelength, lumped-element circuits allow for a much higher degree of miniaturization. This achievement is compensated by higher dissipative losses (large γ_{cond}) and a reduced power handling capability (large γ_{pow}, cf. Sec. 4.1.2). Because of the loss enhancement, lumped-element devices present a unique opportunity to benefit from HTS since normalconducting structures would suffer from untolerably large insertion losses. Besides the advantage of extremely compact low-loss circuits at frequencies f≤10 GHz (guided wavelength ≥ 6 mm for $\varepsilon_r=25$), lumped-element circuits offer the possibility to build synthetic transmission lines with (almost) arbitrary scattering parameters. Presribed pass and stop bands can be synthesized by arranging reactive elements periodically along the transmission line, or by using resonant LC-elements. Because of the possibility to place loosely coupled adjacent cells close to each other, very narrow-band filters can be designed which would require large-area microstrip circuits if built from distributed elements[138]. Furthermore, phase responses can be designed with large group delays within the passband and with presribed frequency dependences[139].

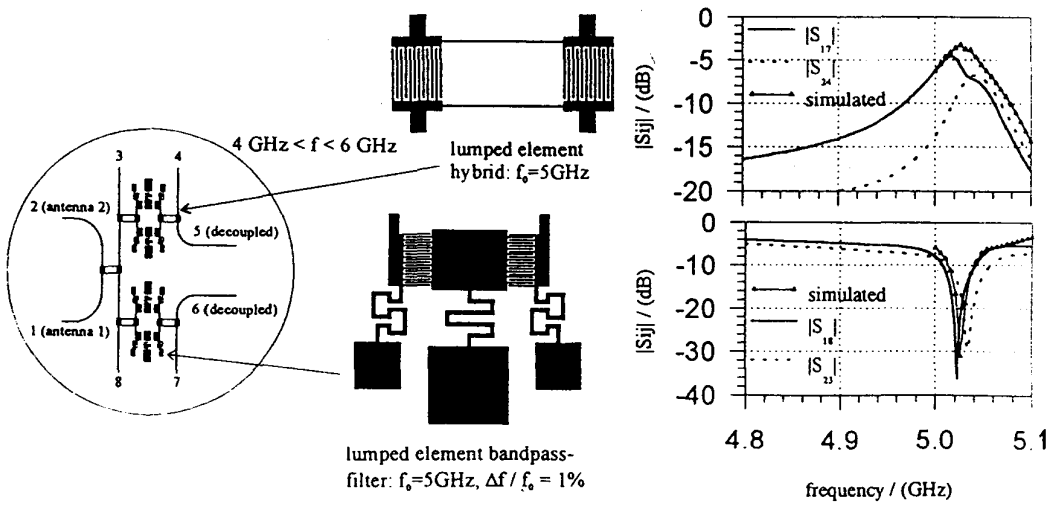

Fig. 15: Layout of a lumped-element Y-123 frequency diplexer at 5 GHz with integrated 3 dB-couplers on 1" LAO (left) and measured and simulated frequency response (right)[144].

Miniaturized HTS bandpass and bandstop[139,140,141] and HTS allpass filters[142] were successfully composed of interdigital and patch capacitors and narrow-strip or loop inductors. Compared to a Cu allpass with an insertion loss of 2 dB at 77 K, less than 0.3

dB (at 3 GHz) and 1 dB (up to 6 GHz) were obtained with Y-123 films on $LaAlO_3$[142]. The allpass section covering an area of 1.5x2.8 mm^2 exhibited a group delay of 0.7 ns at 77 K and 2.8 GHz. Linear response was measured up to a power level of 18 dBm. An HTS coplanar slow-wave structure on MgO was obtained with periodically arranged reactive elements at a unit cell period of 0.4 mm[143]. The length and center frequency of the resonant structure of 1 cm and 1.6 GHz yielded a reduction of the group velocity by a factor of 4 compared to a homogeneous line[141].

Recently, approaches were reported to synthesize more complicated circuits for the receiving stage of mobile communication systems. Fig. 15 shows the layout of a lumped-element circuit consisting of two identical pairs of bandpass filters (center frequency 5 GHz, fractional bandwidth 1%) and three integrated lumped-element hybrid couplers, serving as a frequency diplexer fed by the output of a two-element antenna array[144]. The simulated response of the circuit (Fig. 15) agreed well with measured results obtained with a 1" Y-123 film on $LaAlO_3$. Fig. 16 shows the layout and the frequency response of a narrowband lumped-element 5-pole bandpass filter at 900 MHz on a 2" $LaAlO_3$ substrate. The measured response of a double-sided Y-123 film revealed an insertion loss of 1.2 dB within the passband of fractional width of only 0.27% [115,138].

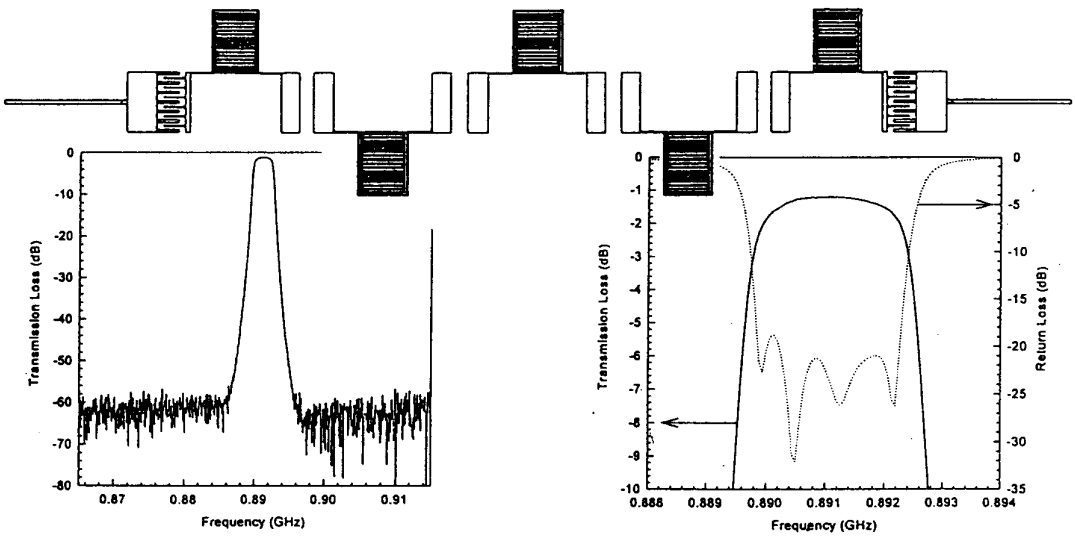

Fig. 16: Layout (top) and frequency response (bottom) of a narrowband lumped-element 5-pole bandpass filter at 900 MHz on a 2" LAO substrate[138]. The separation between the outer edges of the three upright interdigital capacitors corresponds to 1 inch.

4.2.5 Analog tuners and phase-shifters As narrow-bandwidth filters are needed for many potential applications of HTS, tuning becomes an important issue. Considering fractional bandwidths of 1% at frequencies between 1 and 10 GHz means to reproducibly adjust the center frequencies of the filters on a scale of about 100 MHz. Tuning can in principle be performed continuously, either once to adjust a device and keep it fixed, or in-situ by reversible trimming of appropriate circuit parameters. In contrast, switches can be used to achieve programmable device characteristics. Both methods have been investigated for planar HTS components. The results on switched elements, which are based on nonlinear conductivity features of HTS, are discussed in Sec. 4.4.

Continuous adjustment of the phase (or frequency) of microwave devices can be obtained by any means of varying the specific inductance and/or capacitance of the circuit

elements. Besides nonlinear mechanisms based on, e. g., current-induced pair-breaking[145], thermal, electrical and magnetic effects have been investigated. A thermally tuned filter[146,147] provided a tuning range of 10 MHz at 1.4 GHz with an increase of the insertion loss by about 0.7 dB. The microstrip filter contained four switches consisting of narrow Ta film resistors, which were fed by a current. The response time and the power consumption were of the order of 1 to 10 ms and 1 to 10 mW at 77 K, respectively.

Electrical tuning was demonstrated with ferroelectric films deposited onto coplanar lines and onto gaps in microstrip lines[148,149,150]. Applying an electric field gradient affects the permittivity of the ferroelectric and therefore the phase (or resonant frequency) of the HTS circuits. Besides the phase, the characteristic impedance of the line is also affected which leads to a trade-off between tuning and impedance matching. A frequency shift of 300 MHz at a bias voltage of 50 V and a center frequency of 11 GHz were obtained, but the frequency shift was accompanied by an untolerably large increase of the dissipation losses[148]. Recent investigations showed that the tunability increased with increasing thickness of the ferroelectric films while the attenuation stayed almost constant. Phase changes of 8.3^0 of 5 mm long coplanar lines could be induced at 18.5 GHz and 76 K with a bias voltage of 39 V (coresponding to a field gradient of 0.8 MV/m)[149]. While the principle of operation could be demonstrated to be promising, realistic implementation of such tuning elements still relies on the development of suitable ferroelectric materials with a high permittivity and a low loss tangent, and which are compatible with HTS.

Magnetic tuning based on the complex permeability of ferrimagnetic materials is a well known phenomenon[151]. Recently, this effect was also investigated with Y-123 meanderline structures attached to a low-loss ferrite[152]. Differential phase shifts of 700^0 between two extreme polarizations of the ferrite, and an insertion loss below 0.7 dB were measured at 9 GHz for a nonreciprocal arrangement using a YIG torroid. The hyste-retic magnetic properties of the ferrite limited the useful frequency range to values above 5 GHz. Further optimization was stated to involve proper choice of the ferrite material, improved circuit designs and compatibility between the magnetic materials and the HTS films. Recent progress towards a more compact circuit layout and the realization of a 3-element HTS circulator has been reported[153].

Although high-quality HTS filter circuits are already far developed (Secs. 4.2.2 and 4.2.3), reliable tuners need further attention with respect to speed, power dissipation, power consumption, stability of operation and potential for monolithic integration.

4.3 HTS antennas for nuclear magnetic resonance systems

The application of HTS to single radiative elements and to antenna arrays have extensively been reviewed[154,155,156] and retreated in the extended version[2] of this review. Regarding its major potential for short-term commercialization, only one type of HTS antennas will be discussed here.

Nuclear magnetic resonance is a well-known phenomenon in solid state physics, which forms the basis for the investigation of complex multiple-nuclei systems (e. g., Ref. 157). The nuclear spins are oriented by a magnetic field B_0, and then forced to precess by an AC field directed perpendicular to B_0. The frequency of precession, the Larmor frequency ω_0, is related to the DC field B_0 and the nuclear magnetic moment by

$$\omega_0 = \frac{\gamma_{gyr} \cdot B_0}{\mu_0} \quad \text{or} \quad f_0[\text{MHz}] = n_m \frac{e \cdot B_0[\text{T}]}{M_p} \tag{19}$$

with γ_{gyr} the magnetogyric ratio, $n_m=\mu_{nucl}/\mu_K$ the nuclear magnetic moment relative to the nuclear magneton $\mu_K/\mu_0=he/4\pi M_p=5.051\cdot10^{-27}$ J/T, $e=1.602\cdot10^{-19}$ C the elementary charge and $M_p=1.673\cdot10^{-27}$ kg the rest mass of the proton. For important nuclei like ^1H, ^{13}C, ^{14}N and ^{31}P, the n_m-values are 2.792, 0.702, 0.404 and 1.131, which lead to Larmor frequencies between 6.159 and 42.564 MHz per Tesla. Detecting the time dependent precession of a certain nucleus provides important informations on its chemical environment and thus on the structural and dynamic properties of the material under investigation.

Since superconducting magnets with homogeneous fields of several Tesla over extended volumes (cm^3 to m^3) became available, nuclear magnetic resonance has become a basic experimental tool in chemistry and pharmaceutics for the nonradiative high-resolution spectroscopy or microscopy of synthesized molecules (NMR), and in medicine for magnetic resonance imaging (MRI)[158]. The major figure-of-merit in all three cases is the signal-to-noise-ratio, SNR. An improved sensitivity is strongly desired since it allows for a reduced sampling time, which varies as $1/SNR^2$, for an enhanced sample throughput, smaller sample volumes and/or reduced field strengths B_0. These benefits are reflected in system performance and costs, patient comforts and, consequently, in public acceptance. Although the detailed theoretical consideration of the SNR-value is complicated by many input parameters[159,160,161,162], the main results can be summarized in a simplified way:

$$SNR = \frac{F(V_{spl}, V_{rec})\cdot B_1\cdot\omega_0^2}{\Delta f\cdot[\alpha_{rec}(V_{rec})T_{rec}\omega_0 L_{rec}/Q_{rec}+\alpha_{spl}(V_{spl})T_{spl}R_{spl}]^{1/2}} \qquad (20)$$

The subscripts rec and spl stand for the receiving coil and the sample, respectively.

The signal (numerator in Eq. (20)) scales with the filling factor F which depends on absolute values and mutual arrangements of the two volumes V_{spl} and V_{rec}, and with B_1 which describes the magnetic field amplitude per unit current flowing in the coil. Both factors should be as large as possible in an optimized coil design. For the low frequencies of interest ($f_0\leq400$ MHz), the antennas consist of lumped-element receiver coils resonated by appropriately dimensioned capacitors.

There are two major noise contributions (sum under the root in the denominator of Eq. (20)) originating from the sample and the coil, weighted by the parameters α_{rec} and α_{spl}. The noise is usually caused by thermal effects, and it thus scales with the receiving bandwidth Δf and the temperatures of the coil and the sample, T_{rec} and T_{spl}. The coil resistance can be represented by $\omega_0 L_{rec}/Q_{rec}$ with L_{rec} the coil inductance and Q_{rec} its quality factor. The sample resistance R_{spl} can generally be assumed to scale[159,160] as ω_0^2. It should be kept in mind that, for a given nucleus of interest, the frequency is uniquely determined from Eq. (19) by the magnetic field B_0.

It can be seen from Eq. (20) and Fig. 17 that the use of HTS instead of normal-conducting receiver coils is beneficial if the sample resistance is low, i. e. at low frequencies or magnetic fields, or if the sample volume is small. Possible applications concern NMR spectroscopy or microscopy, both of which benefit mostly from reduced sampling times, and low-field MRI ($B_0\leq100$ mT) which enables local rather than whole-body imaging scans. All of these issues have been addressed with the design of planar Tl-2212 and Y-123 coils[163,164,165]. Significant SNR improvements have been achieved: a factor of 4-5 at 25 K in a 400 MHz high-resolution NMR spectrometer[164], up to 8 at 77 K in a 64 mT MRI system[165,166], and up to 10 in a NMR microscope at 10 K[167]. These improvements exceed the performance achievable with cryogenic normalconducting receiver coils and are promising for early commercialization.

Although the progress in this field has been rapid[158], several problems remain challenging. The utilization of HTS implies the use of dewars, which must be optimized

in order not to disturb the magnetic fields B_0 and B_1, not to introduce additional noise sources and not to reduce the filling factor too strongly. Second, the best microwave performance of HTS is achieved with planar patterned thin films, the size of which is presently limited to about 3 inches. The use of polycrystalline material has also been considered[168]. However, granularity leads to untolerably high dissipation losses in elevated magnetic fields (which might be as high as 10 T). Third, the diamagnetic properties of superconductors cause field distortions, which need to be addressed in an optimized design of high-resolution NMR spectrometers. Fourth, high-Q receiver coils limit the receiving bandwidth (Sec. 4.1.1). For Q-values of 10^3 to 10^4 at f_0=3 MHz, the antenna bandwidth falls below 3 kHz while typical MRI systems require some 10 kHz. Therefore, superconductive matching networks and/or tuning circuits have to be designed without an excessive increase of the insertion loss[163]. Finally, if the HTS antenna is designed for receiving as well as for transmitting modes, nonlinear effects as considered in Secs. 2.2.3 and 4.1.2 are expected to limit the achievable performance.

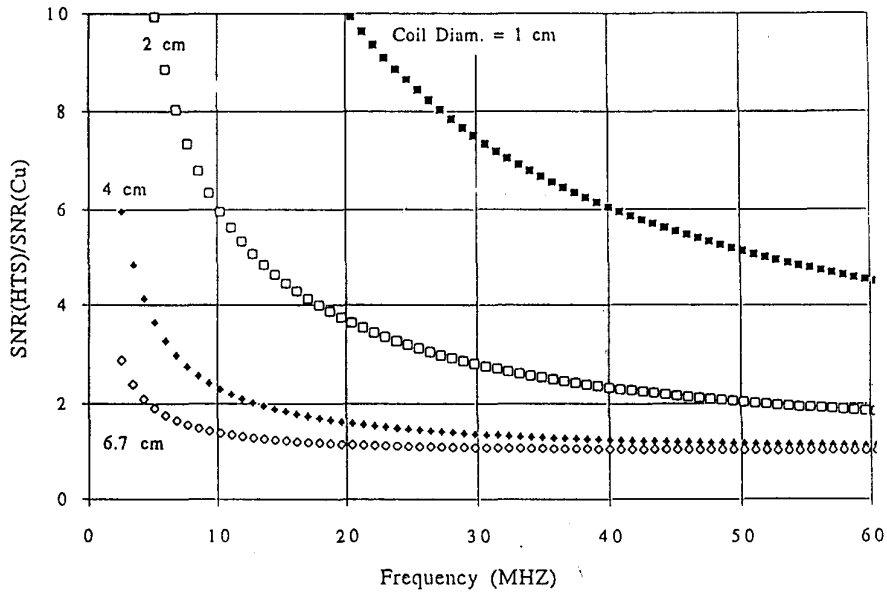

Fig. 17: Conditions for favorable application of HTS receivers in low-field MRI[165].

4.4 Microwave components based on nonlinear effects

In this paragraph, the nonlinear microwave conductivity of HTS is considered for possible applications. Important building blocks are linear time-varying (e. g. switches, modulators, mixers or samplers) or nonlinear devices (e. g. power limiters or pulse formers). Such components can in principle be fabricated in a hybrid HTS-semiconductor technology, but monolithic HTS devices may be advantageous for integrated systems given that their performance could compete with that of present semiconducting devices.

As discussed in Secs. 2.1 and 2.2, nonlinear dynamic effects can be provoked by affecting the thermal or kinetic energy of the superconductor. Accordingly, physical temperature, impressed currents and magnetic fields (from DC to microwave or even optical frequencies) present the experimental keys to access the nonlinear regime. A common method to evoke current-induced nonlinear effects in homogeneous HTS devices is to exploit the current enhancement at the edges of planar microwave structures. Coplanar line-sections for which the characteristic impedance and the current enhancement at the inner conductor can be chosen independently, have mainly been employed.

4.4.1 Switches Switches represent one class of microwave devices which might benefit from the nonlinear dynamic transport processes in HTS[86]. They form key elements in the construction of programmable filter banks or delay lines for spectral analysis. Triggered by a control parameter (e. g., a current), switching between an "on" state with a low insertion loss and an "off" state with high isolation can be obtained. For proper adjustment of the amplitude, sequence and duration of the control current pulses, switching elements provide the basis for modulating or sampling operations.

In most cases, the transition of HTS from the super- (S) to the normalconducting (N) state has been considered for the on- and off- states. Low-frequency currents[169], micro- or nanaosecond microwave pulses[63,170] or femtosecond laser pulses[77,78] were investigated as control parameters (see also Ref. 86 and references therein). The controlled variation of the local temperature of a device segment by means of thermal switches[147] or of the dielectric properties of a layer deposited onto a HTS film by optical signals[171] were also reported. The attainable transmission-to-isolation signal ratio depends on the signal frequency, the operating temperature and the superconductor film thickness (Sec. 2.2.1) and on the device geometry. Besides low and high "on" and "off" signal attenuations, high switching speeds are desirable. Switching times of less than 2 μs and of 80 ps (a few ns) for S-N (N-S) transitions were reported for the current and laser pulse controlled devices, respectively. The thermal switches were much slower (50 and up to 500 ms for S-N and N-S) and highly power consumptive (about 0.1 W).

The reported performance parameters were strongly affected, if not limited, by the experimental setup. However, the time scales inherent to the HTS materials were also investigated by many groups[77,78,170]. A recent analysis of ultimate switching speeds in HTS films can be found in Ref. 170. According to this paper, four time regimes can be separated during the dynamic response. First, heating of the electronic subsystem of the HTS takes place on a time scale $\tau_{e\text{-}p}\approx 1$ ps, which is characteristic for an energy transfer between electrons and phonons, e. g., during recombination of quasiparticles into Cooper pairs[77]. Due to the large difference in specific heat capacities of the electronic system and the lattice, $C_p/C_e\approx 30\text{-}40$, the phonon-electron interaction time (governing, e. g., pair breaking processes) is $\tau_{p\text{-}e}\leq 40$ ps. Third, the time for phonons to escape from the film to the substrate is typically $\tau_{esc}\approx 5$ ns. It is given by the product of the film thickness times the specific heat of the substrate times the thermal boundary resistance between substrate and film. Even longer response times are expected for thermal relaxation processes within the substrate and the complete package. If the duration of the control pulses was adjusted between $\tau_{e\text{-}p}$ and $\tau_{p\text{-}e}$, thermal effects could be completely suppressed. If furthermore small HTS switching volumes and operating temperatures close to T_c were considered, ultimate switching speeds of the order of 100 GHz might be achieved[170] with an average power consumption of about 10 μW. Realistic switching speeds further depend on the "overcriticality" parameter $(I/I_c\text{-}1)$ with I the amplitude of the control signal and I_c the critical current limiting the linear performance of the considered device[172,173].

4.4.2 Mixers and detectors Although the physical origin of the nonlinear dynamic microwave response of HTS is not yet fully understood (e. g. kinetic inductive and/or resistive mechanisms), attempts have been made to construct a HTS mixer based on the fast response employing a pulsed pumpsignal. A prototype for a monolithic HTS second-harmonic mixer was described in Refs. 111,174. In a first step, a normalconducting filter circuit integrated with a HTS nonlinear transmission line element provided a minimum conversion loss of 15 dB at 80 K from a 9 GHz RF signal and a 5 GHz pumpsignal (local oscillator (LO) at +15 dBm power) to an intermediate frequency (IF) of 1 GHz. The

device performance was limited by thermally induced nonlinearities and imperfect matching of the ports to the small dynamic resistance of the HTS element.

The design of HTS resistive mixers can be facilitated if the dynamic current-voltage characteristic of the nonlinear HTS element is considered. Fig. 18 shows such a characteristic for a Y-123 bridge measured at the end of the 200 ps long leading edge of 1 to 10 ns long pulses[173]. Also shown are calculated data on the optimum conversion efficiency K_{opt} and impedance matching of the mixer circuit. Since maximum frequency conversion is only obtained for matched input and output, high conversion efficiencies are achieved at the expense of reduced bandwidths[173,175,176].

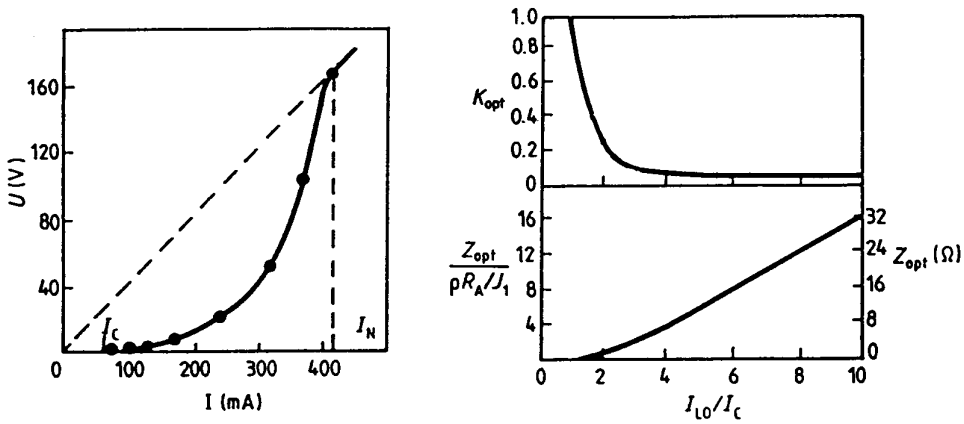

Fig. 18: Dynamic current-voltage characteristic of a Y-123 bridge at the 200 ps long leading edge of a microwave pulse (left) and calculated values for optimum conversion K_{opt} and matched terminal resistances Z_{opt} (right, in reduced and absolute values) versus reduced local oscillator current[173].

Recently, resonant mixer configurations have therefore been proposed[177]. A conversion loss of 8 dB at 77 K and a LO power of 4 dBm was measured for a single-resonant device at 1.85 GHz, which comes already close to the performance of semiconducting devices. Similar approaches towards the development of phase-shifters modulators, limiters and mixers were presented in Refs. 176, 178.

Another possible application of the dynamic nonlinear conductivity of HTS is the detection of millimeter wave or infrared pulses. Successful operation of bolometric as well as non-bolometric HTS photo detectors based on thin YBCO and TBCCO films was reported [77,78,179,180,181]. The responsitivity of bolometric detectors increases proportionally to the steepness of the S-N transition. Therefore, high normal resistance values, e. g. by employing meanderline structures, and small transition widths are required. Guided microwaves were detected at 50 K with 200 to 300 nm thick Y-123 meanders patterned from films on YSZ substrates[181]. Responsitivities of 4 kV/W at 35 GHz and 2.6 kV/W at 70 and 94 GHz were obtained with a bias current of 100 μA. These values have to be compared with typical values of about 1 kV/W available with semiconductor diodes below 100 GHz. Furthermore, no fundamental bandwidth limitation exists for HTS detectors up to the visible regime in contrast to semiconductor devices [180,182].

5 FUTURE PROSPECTS

Regarding the spectrum of aspects considered in the preceding Secs. and the multitude of statements on the future of HTS, which have been quoted earlier, it seems

rather difficult to formulate a comprehensive conclusion. However, since the future of HTS will basically depend on its potential for commercialization, the following Secs. are aimed at evaluating this potential.

5.1 HTS technology: "Status Quo"

5.1.1 Physical and technical achievements As can be concluded from the preceding Secs., the physical understanding of HTS films is far developed (Sec. 2.1). Shortly after the discovery of these materials, rapid progress in film and junction technologies was obtained. The values of surface resistance, penetration depth and critical currents could steadily be improved. Meantime, the rate of (and potential for) further improvements has relaxed. There seems to be a general agreement about the reproducibly achievable performance of the different HTS families at high frequencies, especially the rare earth-123 and Tl-2212 and 2223 compounds (Sec. 2.2). Design tools have been developed and improved, and film deposition, patterning and test facilites were installed at many places. The development of packaging and cooling techniques has, even if delayed and thus more slowly, proceeded to a stage which justifies and, even more, asks for the confrontation with real needs (Sec. 3). Many different single components, passive, analog, linear and nonlinear, were successfully demonstrated (Sec. 4). Time has thus become mature for serious consideration of how these materials could be implemented into useful devices.

One of the major driving forces for focussing the development from single-element circuits to advanced HTS microwave components and subsystems has been the "High-temperature Superconductivity Space Experiment", HTSSE (cf. Tab. 3 and Refs. 3,183,184). Its first phase was devoted to the demonstration of single components with superior performance compared to conventional devices, based on the HTS technology available in 1990. Unfortunately, the complete HTSSE-I-payload, which was successfully assembled, tested and space-qualified on ground, did not receive orbit but was lost. The second phase, using a HTS technology matured within 3 further years, focused on the delivery of complex HTS components and hybrid HTS-seminconductor subsystems. The HTSSE-II-payload contains the HTS devices, cryogenic refrigerators and monitoring electronics (cf. Sec. 3.2.1). The tight time schedules, bound by the satellite launch facilities, forced all contributors to develop materials and packaged devices simultaneously. The payload is expected to be integrated into a satellite during late 1995 and to be launched in summer of 1996 for a one-to-three-years test mission in orbit.

Tab. 3: Reproduction of the time schedule and technological goals of the subsequent phases of the "High temperature superconductivity space experiment", HTSSE[185].

	89	90	91	92	93	94	95	96	97	98	99	00
HTSSE-I												
HTS Devices	———											
Spacecraft Build		———	———									
On-Orbit Mission					X							
HTSSE-II												
HTS Components				———	———							
Spacecraft Build					———	———						
On-Orbit Mission								———	– – – – –			
HTSSE-III												
HTS Systems								?	?	?		
Spacecraft Build												
On-Orbit Mission												

The different contributions to HTSSE II were presented in Refs. 3,184,186 and treated, from a more general point-of-view, in Ref. 86. They might be regarded valuable indicators of the presently achieved state-of-the-art of system complexity and of the most promising directions to proceed further. HTSSE II contains multichannel filter banks, delay lines composed of several building elements and interlaced with integrated amplifiers, low-noise hybrid and cueing receivers (the latter being based on chirp filters, cf. Sec. 4.2.2), a multidimensional antenna array (which is considered for a separate test in space), and a simple digital multiplexer employing HTS Josephson junctions. The final, third phase of HTSSE was originally considered to start between 1995 and 1998. It is aimed at the fabrication of a fully integrated system involving HTS and, eventually, semiconductor microwave devices, with enhanced performance on a system level. Present efforts focus on the identification of such a system for useful application in future generations of satellite systems, which are accounted for by the question marks in Tab. 3.

5.1.2 At the edge of a new market A profound scientific understanding and a reliable technical handling of a new class of materials like the HTS are supposed to be the main prerequisites before serious considerations of possible applications. However, economic concerns put further constraints on a successful commercialization.

First, the superior performance of HTS over conventional components is counter-balanced by the cooling requirements. Single conventional device elements will therefore be replaced by HTS components only if there is no other way to achieve a comparable electrical performance or if the overall system costs can be reduced.

Second, the trade-off between costs and performance will favor the utilization of HTS as more components can simultaneously benefit from the low operating temperature. Since complete monolithically integrated HTS-based microwave systems (containing both passive and active, homogeneous and junction elements) are not yet in sight, hybrid super-semiconducting (HTS-SC) circuits will remain essential ingredients in the future development[111]. Such novel systems will contain components which benefit from the low dissipation losses, the potential for miniaturization and the unique Josephson properties of superconductive elements as well as from enhanced charge carrier mobility, reduced thermal noise and lower power consumption of semiconductor circuits. The advantages of cryogenic SC electronics have therefore extensively been investigated and developed[86,187].

Third, the development of the HTS technology has had to surpass: a) The development of suitable fabrication techniques which encountered the difficulties related with the short coherence length and the pronounced anisotropy, b) the development of reliable, light-weight and cheap cooling systems and c) the identification of economically interesting applications. The advent of relaxed cooling requirements has initiated a re-evaluation of superconductor technology in general, which was known before mainly from medical applications (Sec. 4.3 and Ref. 4).

Finally, the acceptance of a new technology or even novel system architectures is known to depend strongly on the actual trend for innovations. As long as existing systems, e. g., in earth-based or satellite communication systems, operate reliably and without the need for improved performance, novel ideas will hardly penetrate the market. In contrast, if new system generations are to be developed like digital and/or adaptive communication systems, "unconventional" approaches have the chance of being much more seriously considered.

The relevant time scales for a new technology to bear commercial products is expected to be in the range of 20 to 40 years[4]. The HTS technology with its age of 8 years should accordingly be regarded to be still in its infancy. In this context, it might be a valuable indicator for a realistic economic future of HTS in microwave systems that scien-

tific developments are obviously moving from research institutes to companies, and that novel approaches in layout and performance are patented before, if ever, being published.

5.2 HTS technology: "Quo vadis"

5.2.1 Remaining challenges The achieved state-of-the-art of HTS technology is considerable, and the rush for early commercialization plausible. However, in summarizing the challenges quoted in Secs. 2 to 4, several important issues can be identified which deserve further research.

On the material site, the multilayer technology of monolithic HTS or hybrid devices needs further development. Double-sided film deposition, homogeneous oxygenation of HTS base or intermediate layers, the development of insulating, dielectric or cap layers and the invention of novel dielectric materials with high permittivity and low loss tangent need to be pursued. Nonlinear effects at elevated power levels have to be understood better to make linear high-power devices become a reality. The number- and areal densities of defects in epitaxial films and substrates up to 3" in diameter must be considerably reduced before very long delay lines and large-scale integrated (e. g., lumped-element) devices become operational.

On the device site, more research and development are needed for appropriate design tools, e. g., for high-Q multipole filter systems or low-inductance circuits. A very important class of devices which is still under development is fast, low-dissipation and low-noise tuners. Such components are basic, e. g., for tunable filter banks, high-Q dielectric-shielded resonators in stable local oscillators, adaptive and phased-array antenna systems. Furthermore, as far as the low impedances of superconductive microwave circuits are concerned, low-loss matching networks are required for maximum bandwidth. Further issues, which are of special concern for application of HTS in satellite systems, were discussed in Ref. 3.

A very exciting feature associated with the research on HTS has been the revival of cooler development. The actual achievements are impressive, but a lot remains to be done. Reliable (MTBF$\geq 10^4$ h), light-weight ($\leq$5 kg), efficient ($\eta_c \geq 0.1$) and cheap ($\leq 10^3$ US$) CCCs with improved vibrational performance should be the goals.

Finally, as HTS have become an important part of today´s high-technologies, novel system architectures should be envisaged. The demand for higher capacities and information densities and less stringent power requirements in wireless communication systems present an ideal chance for HTS to provide unique solutions which would not have become possible otherwise. Ingenious and, maybe, at first glance unconventional, ideas need to be pursued in order to exploit the full potential of these new materials. Anticipating further improvements in cooling systems, hybrid oxide and metallic superconductor systems operating at intermediate temperatures around 20 K, e. g. for LTS digital signal processing in HTS receivers, might become also conceivable.

5.2.2 Projected market development The speed and the success of developing new technologies result from a balance between the required (technical and financial) efforts and the projected payoffs. Projections of future market developments may therefore serve as an important driving force and/or as a political instrument to facilitate further developments. The quantitative estimation of possible market sales is from its nature uncertain. Different predictions of the future of HTS were published[188,189,190,191,192]. While the actual sales numbers and time scales differ for these analyses, they have in common that HTS microwave systems are most likely to be implemented in wireless communication systems, either in earth-based cell sites of mobile phone systems[193,194,195] or in

satellite-based communication links and advanced navigation systems. Furthermore, medical systems are likely to benefit from HTS components, e. g., in MRI receivers (Sec. 4.3) and novel margnetocardiography systems[2]. According to the time scale mentioned before, market penetration of electronics systems is expected to occur with the upcoming millenium. Growth rates of the market sales by a factor of 4 to 10 per decade are then predicted, reaching in 2020 a level between 120 and 200 billions US$ per year for all types of superconducting systems world-wide. Electronic and medical systems are expected to contribute by about 50% to this number.

Though we cannot foresee all possible adventures of the future development of HTS, the next generation of physicists and engineers will still have the pleasure to participate in an extremely challenging technology, as has had the present generation.

ACKNOWLEDGMENTS

Valuable contributions from my colleagues at the University of Wuppertal are highly appreciated. Special thanks belong to Heinz Chaloupka, Günter Müller and Helmut Piel for contributing important ideas and stimulating discussions. Many collaborators from institutes all over the world have made this review possible by providing actual results and relevant informations, partially prior to publication. Final thanks are devoted to God for the gifts of patience and faith with which my family supported the preparation of this review.

REFERENCES

1. N. Newman and W. G. Lyons, J. Supercond. **6**, 119 (1993) and N. Newman, in: "High-Temperature Superconductors", J. J. Pouch, S. A. Alterovitz, R. R. Romanofsky Eds., (TransTech. Publ., Switzerland, 1994).
2. M. A. Hein, in: "Studies of High-temperature superconductors", Vol. 18, A. Narlikar Ed., (Nova Science, New York, 1996).
3. G. W. Mitschang, IEEE Trans. Appl. Supercond. **5**, 69 (1995).
4. H. Piel, Keynote Contrib. 2nd Europ. Conf. Appl. Supercond., EUCAS, July 2-6, 1995, Edinburgh, Scotland.
5. J. Halbritter, Z. Phys. **266**, 209 (1974).
6. R. Blaschke and R. Blocksdorf, Z. Phys. **B49**, 99 (1982).
7. C. Kittel, Quantum Theory of Solids, (Wiley, New York, 1963).
8. J. R. Waldram, Adv. Phys. **13**, 1 (1964).
9. C. J. Gorter and H. Casimir, Phys. Z. **35**, 963 (1934).
10. D. A. Bonn, R. Liang, T. M. Riseman, D. J. Baar, D. C. Morgan, K. Zhang, P. Dosanjh, T. L. Duty, A. MacFarlane, G. D. Morris, J. H. Brewer, W. N. Hardy, Phys. Rev.**B47**, 11314 (1993).
11. A. M. Portis: "Electrodynamics of high-temperature superconductors", Lecture Notes in Physics, Vol. 48 (World Scientific, Singapore, 1993).
12. U. Dähne, N. Klein, H. Schulz, N. Tellmann, K. Urban, Contrib. 2nd Europ. Conf. Appl. Supercond., EUCAS, July 2-6, 1995, Edinburgh, Scotland.
13. Ya. G. Ponomarev, B. A. Aminov, N. B. Brandt, M. A. Hein, C. S. Khi, V. Z. Kresin, G. Müller, H. Piel, K. Rosner, S. V. Thesnokov, E. B. Tsokur, D. Wehler, K. Winzer, Th. Wolf, A. V. Yarygin, K. T. Yusupov, Phys. Rev. **B 52**, 1352 (1995).
14. D. A. Bonn, S. Kamal, Kuan Zhang, Ruixing Liang, D. J. Baar, E. Klein, W. N. Hardy, Phys. Rev. **B 50**, 4051 (1994).
15. G. Müller, N. Klein, A. Brust, H. Chaloupka, M. Hein, S. Orbach, H. Piel, D. Reschke, J. Supercond. **3**, 235 (1990).
16. M. R. Beasley, Physica C **185-189**, 227 (1991).
17. Z. X. Shen, D. S. Dessau, B. O. Wells, D. M. King, W. E. Spicer, A. J. Arko, D. Marshall, L. W. Lombardo, A. Kapitulnik, P, Dickinson, S. Doniach, J. DiCarlo, A. G. Loeser, C. H. Park, Phys. Rev. Lett. **70**, 1553 (1993).

18. J. Kane, Chen Qun, K. W. Ng, H. J. Tao, Phys. Rev. Lett. **72**, 128 (1994).
19. B. A. Aminov, B. Aschermann, M. A. Hein, F. Hill, M. Lorenz, G. Müller, H. Piel, Phys. Rev. **B 52**, 1. Nov. (1995).
20. N. Klein, N. Tellmann, H. Schulz, K. Urban, S. A. Wolf, V. Z. Kresin, Phys. Rev. Lett. **71**, 3355 (1993).
21. S. Orbach-Werbig, Dissertation WUB-DIS 94-9, Univ. of Wuppertal (1994).
22. G. Liang, Proc. 6thWorkshop on RF Superconductivity, R. M. Sundelin Ed., Continuous Electron Beam Accelerator Facility, CEBAF, Newport News, Virginia, USA, 307 (1993).
23. G. Müller, Proc. 4th Workshop on RF Superconductivity, Y. Kojima Ed., KEK Report 89-21, KEK, Tsukuba, Japan (1990), 267.
24. N. Klein, Proc. 5th Workshop on RF Superconductivity, D. Proch Ed., DESY M-92-01, Deutsches Elektronen Synchrotron, Hamburg, Germany (1992), 285.
25. N. Klein, H. Chaloupka, G. Müller, S. Orbach, H. Piel, B. Roas, L. Schultz, U. Klein, M. Peiniger, J. Appl. Phys. **67**, 6940 (1990).
26. A. Porch, J. R. Powell, M. J. Lancaster, J. A. Edwards, R. G. Humphreys, IEEE Trans. Appl. Supercond. **3**, 1987 (1995).
27. N. Klein, U. Poppe, N. Tellmann, H. Schulz, W. Evers, U. Dähne, K. Urban, IEEE Trans. Appl. Supercond. **3**, 1102 (1993).
28. S. M. Anlage, B. W. Langley, G. Deutcher, J. Halbritter, M. R. Beasley, Phys. Rev. **B 44**, 9764 (1991).
29. S. M. Anlage and D. H.Wu, J. Supercond. **5**, 395 (1992).
30. S. Orbach, S. Hensen, G. Müller, H. Piel, M. Lippert, G. Saemann-Ischenko, S. A. Wolf, J. Alloys & Compounds **195**, 555 (1993).
31. V. Z. Kresin and S. A. Wolf, Phys. Rev. **B 46**, 6458 (1992) and
V. Z. Kresin, H. Morawitz and S. A. Wolf: "Mechanisms of conventional and high-T_c superconductivity", (Oxford University Press, New York, 1993).
32. S. Hensen, S. Orbach-Werbig, G. Müller, H. Piel, N. G. Chew, J. A. Edwards, R. G. Humphreys, in: "Applied Superconductivity", H. C. Freyhardt Ed. (DGM Informationsgesellschaft, Oberursel, 1993), 1053.
33. N. G. Chew, J. A. Edwards, R. G. Humphreys, J. S. Satchell, S. W. Goodyear, B. Dew, N. J. Exon, S. Hensen, M. Lenkens, G. Müller, S. Orbach-Werbig, IEEE Trans. Appl. Supercond. **5**, 1167 (1995).
34. J. Mao, D. H.Wu, J. L. Peng, R. L. Greene, S. M. Anlage, Phys. Rev. **B51**, 3316 (1995).
35. R. C. Taber, P. Merchant, R. Hiskes, S. A. DiCarolis, M. Narbutovskih, J. Supercond. **5**, 371 (1992).
36. J. P. Turneaure, J. Halbritter, H.A. Schwettmann, J. Supercond. **4**, 341 (1991).
37. A. Gladun, N. Cherpak, A. Gippius, S. Hensen, M. Lenkens, G. Müller, S. Orbach, H. Piel, Cryogenics, **32**, 1071 (1992).
38. T. Jacobs, S. Sridhar, C. T. Rieck, K. Scharnberg, T. Wolf, J. Halbritter, J. Phys. Chem. Solids (1995).
39. P. A. Lee, Phys. Rev. Lett. **71**, 1887 (1993).
40. P. J. Hirschfeld, W. O. Puttika, D. J.Scalapino, Phys. Rev. Lett. **71**, 3705 (1993).
41. M. Prohammer and J. P.Carbotte, Phys. Rev. **B43**, 5370 (1991).
42. S. Orbach-Werbig, A. Golubov, S. Hensen, G. Müller, H. Piel, Physica **C 235-240**, 1823 (1994).
43. A. Porch, M. J. Lancaster, R. G. Humphreys, N. G. Chew, IEEE Trans. Appl. Supercond. **3**, 1719 (1993).
44. W. L. Holstein, L. A. Parisi, Z. Y. Shen, C. Wilker, M. S. Brenner and J. S. Martens, J. Supercond. **6**, 191 (1993).
45. M. A. Hein, F. Hill, G. Müller, H. Piel, H. P. Schneider, M. Strupp, IEEE Trans. Appl. Supercond. **3**, 1745 (1993) and
M. A. Hein, Dissertaion WUB-DIS 92-2, University of Wuppertal (1992).
46. U. Welp, W. K. Kwok, G. W. Crabtree, K. G. Vandervoort, J. Z. Liu, Phys. Rev. Lett. **62**, 1908 (1989).
47. M. A. Hein, M. Strupp, H. Piel, A. M. Portis, R. Gross, J. Appl. Phys. **75**, 4581 (1994).
48. D. H. Wu and S. Sridhar, Phys. Rev. Lett. **65**, 2074 (1990).
49. M. Golosovsky, M. Tsindlekht, H. Chayet, D. Davidov, Phys. Rev. **B**, 470 (1994).

50. D. H. Wu, J. C. Booth, S. M. Anlage, Phys. Rev. Lett. **75**, 525 (1995).
51. J. C. Booth, D. H. Wu, S. M. Anlage, in: "High-Temperature Microwave Superconductors and Applications", J. Hodge Ed., Proc. SPIE **2559** (1995).
52. B. Parks, S. Spielman, J. Orenstein, D. T. Nemeth, F. Ludwig, J. Clarke, P. Merchant, D. J. Lew, Phys. Rev. Lett. **74**, 3265 (1995).
53. I. S. Gosh, L. F. Cohen, V. Frey, T. Tate, A. D. Caplin, J. C. Gallop, S. Sievers, R. Somekh, S. Hensen, M. Lenkens, IEEE Trans. Appl. Supercond. **5**, 1756 (1995).
54. C. Wilker, Z. Y. Shen, P. Pang. W. L. Holstein, D. W. Face, IEEE Trans. Appl. Supercond. **5**, 1665 (1995).
55. M. Hein, S. Hensen, G. Müller, S. Orbach, H. Piel, M. Strupp, N. G. Chew, J. A. Edwards, S. W. Goodyear, J. S. Satchell, R. G. Humphreys, in: "High-temperature superconductor thin films", L. Correra Ed., (Elsevier, North Holland, 1992), 95.
56. W. Diete, B. Aschermann, H. Chaloupka, M. Jeck, T. Kamppeter, S. Kolesov, G. Müller, H. Piel, H. Schlick, Contrib. 2nd Europ. Conf. Appl. Supercond., EUCAS, July 2-6, 1995, Edinburgh, Scotland.
57. G. Müller, B. Aschermann, H. Chaloupka, W. Diete, M. Getta, M. Hein, S. Hensen, F. Hill, M. Lenkens, S. Orbach-Werbig, T. Patzelt, H. Piel, J. Rembesa, H.Schlick, T. Unshelm, R. Wagner, IEEE Trans. Appl. Supercond. **5**, 1729 (1995).
58. N. Klein, N. Tellmann, U. Dähne, A. Scholen, H. Schulz, G. Höfer, H. Kratz, IEEE Trans. Appl. Supercond. **5**, 2663 (1995).
59. A. Porch, M. J. Lancaster, R. G. Humphreys, IEEE Trans. Microwave Theory Tech. **43**, 306 (1995).
60. B. Avenhaus, A. Porch, M. J. Lancaster, S. Hensen, M. Lenkens, S. Orbach-Werbig, G. Müller, U. Dähne, N. Tellmann, N. Klein, C. Dubourdieu, J. P. Senateur, O. Thomas, H. Karl, B. Stritzker, IEEE Trans. Appl. Supercond. **5**, 1737 (1995).
61. W. Rauch, E. Gornik, G. Sölkner, A. A. Valenzuela, F. Fox, H. Behmer, J. Appl. Phys. **73**, 1866 (1993).
62. U. Salz, S. Hofschen, R. Schneider, IEEE Trans. Appl. Supercond. **3**, 2816 (1993).
63. H. Chaloupka, M. Jeck, S. Kolesov, O. Vendik, Proc. 22nd Europ. Microwave Conf., Helsinki, (1992), 189.
64. T. Yoshitake, H. Tsuge, T. Inui, IEEE Trans. Appl. Supercond. **5**, 2571 (1995).
65. B. A. Willemsen, J. S. Derov, J. H. Silva, S. Sridhar, IEEE Trans. Appl. Supercond. **5**, 1753 (1995).
66. A. Andreone, C. Cantoni, A. Cassinese, A. DiChiara, Contrib. 2nd Europ. Conf. Appl. Supercond., EUCAS, July 2-6, 1995, Edinburgh, Scotland.
67. O. Vendik and E. Kollberg, Microwave & RF **7**, 118 (1993).
68. D. E. Oates, P. P. Nguyen, G. Dresselhaus, M. S. Dresselhaus, G. Koren, E. Polturak, to be published in J. Supercond.
69. H. Chaloupka et al., to be published.
70. A. Porch, M. J. Lancaster, R. G. Humphreys, N. G. Chew, J. Alloys & Compounds **195**, 563 (1993).
71. P. P. Nguyen, D. E. Oates, G. Dresselhaus, M. S. Dresselhaus, Phys. Rev. **B 48**, 6400 (1993).
72. M. Manzel, S. Huber, H. Bruchlos, M. Köhler, W. Diete, S. Hensen, G. Müller, J. Keppler, C. Neumann, M. Klauda, Contrib. 2nd Europ. Conf. Appl. Supercond., EUCAS, July 2-6, 1995, Edinburgh, Scotland.
73. W. L. Holstein, Z. Y. Shen, C. Wilker, D. W. Face, D. J. Kountz, in: "Advances in Superconductivity V", (Springer, Tokyo, 1993).
74. R. W. Ralston, D. E. Oates, A. C. Anderson, W. G. Lyons, Extended Abstracts of the 4th Internat. Conf. Supercond. Electronics, ISEC '93, Boulder, 48 (1993).
75. A. Porch, B. Avenhaus, F. Wellhöfer, P. Woodall, Contrib. 2nd Europ. Conf. Appl. Supercond., EUCAS, July 2-6, 1995, Edinburgh, Scotland.
76. A. Ghis, S. Pfister, J. C. Villegier, M. Nail, J. P. Maneval, IEEE Trans. Appl. Supercond. **3**, 2136 (1993).
77. M. A. Heusinger, A. D. Semenov, R. S. Nebosis, Y. P. Gousev, K. F. Renk, IEEE Trans. Appl. Supercond. **5**, 2595 (1995).
78. F. Hegmann, D. Jacobs-Perkins, S. H. Moffat, C. C. Wang, R. A. Hughes, M. Currie, P. M. Fauchet, T. Y. Hsiang, J. S. Preston, R. Sobolewski, Appl. Phys. Lett. **67**, 285 (1995).

79. C. W. Lam, D. M. Sheen, S. M. Ali, D. E. Oates, IEEE Trans. Appl. Supercond. **2**, 58 (1992).
80. T. L. Hylton, A. Kapitulnik, M. R. Beasley, J. P. Carini, L. Drabeck, G. Grüner, Appl. Phys. Lett. **53**, 1343 (1988).
81. J. Halbritter, J. Appl. Phys. **68**, 6315 (1990).
82. C. Attanasio, L. Maritato, R. Vaglio, Phys. Rev. **B43**, 6128 (1991).
83. P. P. Nguyen, D. E. Oates, G. Dresselhaus, M. S. Dresselhaus, A. C. Anderson, Phys. Rev. **B 51**, 6686 (1995).
84. J. S. Herd, J. Halbritter, K. G. Herd, IEEE Trans. Appl. Supercond. **5**, 1991 (1995).
85. R. W. Röth, H. G. Kürschner, G. Müller, H. Piel, D. Reschke, Proc. 3rd Europ. Particle Accelerator Conf., EPAC 92, (Edition Frontières, Gif-sur-Yvette, 1992), ISBN 2-86332-115-3, 1325.
86. Zhi-Yuan Shen: "High-temperature superconducting microwave circuits", (Artech House, Boston, London, 1994).
87. R. F. Barron, "Cryogenic systems", (Oxford University Press, London, 1985).
88. T. P. Sheahen: "Introduction to High-Temperature Superconductivity", (Plenum Press, New York, 1994).
89. P. J. Kerney and M. Nisenoff, Cryogenics **35**, 405 (1995).
90. M. Nisenoff, in: "Cryocoolers 8", R. G. Ross, Jr., Ed., (Plenum Press, New York, 1995), 913.
91. R. A. Ackermann, Superconductor Industry **6**, 15 (1993).
92. G. Kaiser, M. Thürk, P. Seidel, Adv. Cryo. Eng. **40** (1995); **39**, 1281 (1993).
93. G. Thummes, R. Landgraf, F. Giebeler, M. Mück, C. Heiden, Proc. Cryogenic Eng. Conf., CEC/ICMC, Columbus, Ohio, July 17-21, 1995.
94. See, e. g., contributions to "Cryocoolers 8", R. G. Ross, Jr., Ed., (Plenum Press, New York, 1995) and Proc. of the 15th Internat. Cryogenic Eng. Conf., Cryogenics **34** (1994).
95. R. A. Byrns, Proc. 4th Workshop on RF Superconductivity, Y. Kojima Ed., KEK Report 89-21, KEK, Tsukuba, Japan, 329 (1990).
96. D. Proch and C. H. Rode, Proc. 5th Workshop on RF Superconductivity, D. Proch Ed., DESY M-92-01, Deutsches Elektronen Synchrotron, Hamburg, Germany, 1049 (1992).
97. A. Matlashov, Y. Zhuravlev, V. Slobodchikov, N. Bondarenko, A. Bakharev, D. Rassi, Proc. 9th Intern. Conf. Biomagn., August 1993, Vienna, Austria.
98. A. Cochran, G. B. Donaldson, L. N. C. Morgan, R. M. Bowman, K. J. Kirk, Brit. J. NDT **35**, 173 (1993).
99. R. Radebaugh, Jap. J. Appl. Phys. **26**, Supplement 26-3, 2076 (1987) and Adv. Cryo. Eng. **35**, 1191 (1990).
100. M. Wilson, Superconductor Industry **6**, 30 (1993).
101. W. E. Gifford and R. Longsworth, Adv. Cryo. Eng. **10 B**, 69 (1965).
102. E. I. Mikulin, A. A. Tasarov, M. P. Shkrebyonock, Adv. Cryo. Eng. **29**, 629 (1984).
103. S. Zhu and P. Wu, Cryogenics **30**, 514 (1990).
104. G. Thummes, F. Giebeler, C. Heiden, in "Cryocoolers 8", R. G. Ross, Jr., Ed., (Plenum Press, New York, 1995), 383.
105. Y. Matsubara and J. L. Gao, Cryogenics **34**, 259 (1994).
106. C. Heiden, Univ. Gießen, Germany, private communication (1995).
107. M. Nisenoff, S. A. Wolf, J. C. Ritter and G. Price, Physica **C 209**, 263 (1993).
108. T. Kawecki, D. R. Mahony, S. S. Chappie, Proc. Space Cryogenics Workshop, 1995.
109. Y. Nagai, ISTEC Journal **7**, 36 (1994).
110. C. C. Wang, M. Currie, D. Jacobs-Perkins, R. Sobolewski, T. Y. Hsiang, M. J. Feldman, Contrib. 2nd Europ. Conf. Appl. Supercond., EUCAS, July 2-6, 1995, Edinburgh, Scotland.
111. H. J. Chaloupka, M. A. Hein, G. Müller, in: "High-T_c Microwave Superconductors and Applications", R. B. Hammond and R. S. Withers Eds., Proc. SPIE **2156**, 36 (1994).
112. M. Kuhn, R. Horn, A. Baranyak, M. Stiller, M. Klinger, J. H. Hinken, Proc. Workshop on Space Applications of High-Temperature Superconductors, 27.-28. April 1993, ESTEC, Nordwijk, The Netherlands, M. Guglielmi and E. Armandillo Eds., ESA WPP-052 (1993), 93.
113. B. Gurzinski, M. Jeck, H. Chaloupka, Univ. Wuppertal, Germany, private communication.
114. R. C. Taber, J. N. Hollenhorst, L S. Cutler, T. L. Bagwell, N. Newman, B. F. Cole, IEEE Trans. Ultrason. Ferroelectr. Frequ. Control **39**, 398 (1992).

115. G. C. Liang, D. Zhang, C. F. Shih, M. E. Johansson, R. S. Withers, D. E. Oates, A. C. Anderson, P. Polakos, P. Mankiewich, E. de Obaldia, R. E. Miller, to be published in IEEE Trans. Microw. Theory Tech. (1995) and
D. Zhang, G. C. Liang, C. F. Shih, M. E. Johansson, Z. H. Lu, R. S. Withers, to be published in IEEE Trans. Appl. Supercond. (1995).
116. S. J. Hedges and R. G. Humphreys, Electronics Lett. **27**, 2311 (1991).
117. S. J. Hedges and R. G. Humphreys, Proc. 24th Europ. Microw. Conf., Cannes, 517 (1994).
118. F. Huang, H. C. H. Cheung, M. J. Lancaster, R. G. Humphreys, N. G. Chew, S. W. Goodyear, IEEE Trans. Appl. Supercond. **3**, 2778 (1993).
119. G. J. Höfer and H. A. Kratz, in: "Applied Superconductivity", H. C. Freyhardt, Ed., (DGM Informationsgesellschaft, Oberursel, 1993), 1517.
120. G. C. Liang, D. Zhang, C. F. Shih, M. E. Johannson, R. S. Withers, A. C. Anderson, D. E. Oates, IEEE Trans. Appl. Supercond. **5**, 2652 (1995).
121. Y. Nagai, D. F. Hebert, T. vanDuzer, N. Suzuki, O. Michikami, Jap. J. Appl. Phys. **32**, 5527 (1993) and
T. Hayashi, T. Mikazuki, N. Suzuki, Y. Nagai, Electron. Lett. **30**, 1424 (1994).
122. A. Enokihara, K. Mizuno, K. Setsune, Proc. Asia-Pacific Microwave Conf., Japan, 1073 (1995).
123. G. C. Liang, R. S. Withers, B. F. Cole, S. M. Garrison, M. E. Johansson, W. S. Ruby, W. G. Lyons, IEEE Trans. Appl. Supercond. **3**, 3037 (1993).
124. D. E. Oates, MIT Lincoln Laboratory, private communication.
125. G. C. Liang, C. F. Shih, R. S. Withers, B. F. Cole, M. E. Johansson, L. P. Suppan, IEEE MTT-S Digest, 1413 (1993).
126. M. Biehl, A. Vogt, R. Herwig, M. Neuhaus, E. Crocoll, R. Lochschmied, T. Scherer, W. Jutzi, H. Kratz, P. Berberich, H. Kinder, IEEE Trans. Appl. Supercond. **5**, 2279 (1995).
127. W. G. Lyons, R. S. Withers, J. M. Hamm, A. C. Anderson, P. M. Mankiewich, M. L. O'Malley, R. E. Howard, IEEE Trans. Magn. **27**, 2932 (1991).
128. J. Krupka, R. G. Geyer, M. Kuhn, J. H. Hinken, IEEE Trans. Microwave Theory Techn. **42**, 1886 (1994).
129. N. Klein, N. Tellmann, C. Zuccaro, P. Swiatek, H. Schulz, Contrib. 2nd Europ. Conf. Appl. Supercond., EUCAS, July 2-6, 1995, Edinburgh, Scotland.
130. Z. Y. Shen, C. H. Wilker, P. Pang, W. L. Holstein, D. Face, D. J. Kountz, IEEE Microw. Theory Tech. **40**, 2424 (1992).
131. N. Tellmann, N. Klein, U. Dähne, A. Scholen, H. Schulz, H. Chaloupka, IEEE Trans. Appl.Supercond. **4**, 143 (1994).
132. N. Klein, C. Zuccaro, U. Dähne, H. Schulz, N. Tellmann, R. Kutzner, A. G. Zaitsev, R.Wördenweber, J. Appl. Phys. (1995).
133. C. Wilker, Z. Y. Shen, V. X. Nguyen, M. S. Brenner, IEEE Trans. Appl. Supercond. **3**, 1457 (1993).
134. "Dielectric Resonators", D. Kajfez and P. Guillon Eds., (Artech House, Dedham, 1986).
135. Y. Kobayashi and S. Tanaka, IEEE Trans. Microwave Theory Tech. **28**, 1077 (1980).
136. V. L. Gurevich and A. K. Tagantsev, Adv. Phys. **40**, 719 (1991).
137. R. R. Mansour, Van Dokas, G. Thomson, W. C. Tang, C. M. Kudsia, IEEE Trans. Microw. Theory Tech. **42**, 2472 (1994).
138. D. Zhang, G. C. Liang, C. F. Shih, M. J. Johansson, R. S. Withers, to be published in IEEE Trans. Microw. Theory Tech. (1995).
139. T. Patzelt, B. Aschermann, H. Chaloupka, U. Jagodzinski, G. Gieres, B. Roas, in: "Applied Supercond.", H. C. Freyhardt Ed. (DGM Informationsgesellschaft, Oberursel, 1993), 991.
140. M. J. Lancaster, J. Li, A. Porch, N. G. Chew, Electron. Lett. **29**, 1728 (1993).
141. M. J. Lancaster, F. Huang, H. Cheung, J. C. L. Li, A. Gorur, A. Porch, B. Avenhaus, P. Woodall, F. Wellhofer, R. G. Humphreys, N. G. Chew, Proc. HTSED Workshop on HTS Electron Devices, May 26-28 1994, Whistler, Canada.
142. T. Patzelt, B. Aschermann, H. Chaloupka, U. Jagodzinski, B. Roas, Electron. Lett. **29**, 1578 (1993).
143. J. S. Hong and M. J. Lancaster, IEEE Microwave and Guided Wave Lett. **5**, 87 (1995) and
J. S. Hong, M. J. Lancaster, A. Porch, B. Avenhaus, P. Woodall, F. Wellhöfer, Contrib. 2nd Europ. Conf. Appl. Supercond., EUCAS, July 2-6, 1995, Edinburgh, Scotland.

144. T. Unshelm, B. Aschermann, H. Chaloupka, G. Müller, T. Patzelt, H. Schlick, Contrib. 2nd Europ. Conf. Appl. Supercond., EUCAS, July 2-6, 1995, Edinburgh, Scotland and M. A. Hein, B. Aschermann, H. Chaloupka, T. Patzelt, H. Piel, H. Schlick, R. Theisejans, T. Unshelm, R. Wagner, Internal Report, Cryoelectra GmbH, Wuppertal, Germany (1995).
145. S. M. Anlage, H. J. Snortland, M. R. Beasley, IEEE Trans. Magn. **MAG-25**, 1388 (1989).
146. Y. Nagai, Contrib. 2nd Europ. Conf. Appl. Supercond., EUCAS, July 2-6, 1995, Edinburgh, Scotland.
147. Y. Nagai, N. Suzuki, O. Michikami, IEICE Trans. Electron. **E77C**, 1229 (1994).
148. J. A. Beall, R. H. Ono, D. Galt, J. C. Price, IEEE MTT-S Digest, 1421 (1993).
149. D. C. DeGroot, J. A. Beall, R. B. Marks, D. A. Rudman, IEEE Trans. Appl. Supercond. **5**, 2272 (1995) and D. Galt, J. C. Price, J. A. Beall, T. E. Harvey, IEEE Trans. Appl. Supercond. **5**, 2575 (1995).
150. O. G. Vendik, E. Kollberg, S. S. Gevorgian, A. B. Kozyrev, O. I. Soldatenkov, Electron. Lett. **31**, 654 (1995).
151. B. Lax and K. J. Button: "Microwave Ferrites and Ferrimagnetics", (McGraw-Hill, New York, 1962).
152. G. F. Dionne, D. E. Oates, T. H. Temme, IEEE Trans. Appl. Supercond. **5**, 2083 (1995).
153. G. F. Dionne, D. E. Oates, D. H. Temme, J. A. Weiss, to be published in IEEE Microw. Theory Tech. (1996).
154. R. J. Dinger, J. Supercond. **3**, 287 (1990).
155. R. C. Hansen, IEEE Trans. Aerosp. Electron. Syst. **26**, 345 (1990).
156. H. Chaloupka, J. Supercond. **5**, 403 (1992).
157. Ch. Kittel, "Introduction to Solid State Physics (dt.)", (R. Oldenbourg, München, 1988).
158. R. Simon, Superconductor Industry **8** (2), 18 (1995).
159. W. A. Edelstein, G. H. Glover, C. J. Hardy, R. W. Redington, Magn. Res. Med. **3**, 604 (1986).
160. D. I. Hoult and P. C. Lauterbur, J. Magn. Reson. **34**, 425 (1979).
161. D. I. Hoult and R. E. Richards, J. Magn. Reson. **24**, 71 (1976).
162. Z. H. Cho, C. B. Ahn, S. C. Juh, H. K. Lee, R. E. Jacobs, S. Lee, J. H. Yi, J. M. Jo, Med. Phys. **15**, 815 (1988)
163. R. S. Withers, B. F. Cole, M. E. Johannson, G. C. Liang, G. Zaharchuk, in: "High-T_c Microwave Superconductors and Applications", R. B. Hammond and R. S. Withers Eds., Proc. SPIE **2156**, 27 (1994).
164. R. S. Withers, G. C. Liang, B. F. Cole, M. Johansson, IEEE Trans. Appl. Supercond. **3**, 2450 (1993) and W. H. Wong, R. S. Withers, R. Nast, V. Kotsubo, M. E. Johansson, H. D. W. Hill, L. F. Fuks, K. A. Delin, B. Cole, A. L. Brooke, W. W. Brey, A. Barfknecht, W. A. Anderson, Proc. Cryo. Eng. Conf., Columbus, OH, July 1995.
165. J. G. vanHeteren, T. W. James, L. C. Bourne, Magn. Res. Med. **32**, 396 (1994).
166. H. Okada, T. Hasegawa, J. G. van Heteren, L. Kaufman, J. Magn. Reson. **107**, 158 (1995).
167. R. D. Black, T. A. Early, P. B. Roemer, O. M. Mueller, A. Mogro-Campero, L. G. Turner, G. A. Johnson, Science **259**, 793 (1993).
168. A. E. R. Centeno, P. S. Excell, T. W. Button, N. McN.Alford, IEEE Trans. Appl. Supercond. **5**, 19 (1995).
169. B. Avenhaus, A. Porch, F. Huang, M. J. Lancaster, P. Woodall, F. Wellhöfer, Electron. Lett. **31**, 985 (1995).
170. B. Karasik, I. I. Milostnaya, M. A. Zorin, A. I. Elantev, G. N. Gol´tsman, E. M. Gershenzon, IEEE Trans. Appl. Supercond. **5**, 3042 (1995).
171. E. R. Soares, K. F. Raihn, N. O. Fenzi, G. L. Matthaei, IEEE Trans. Appl. Supercond. **5**, 2276 (1995).
172. L. G. Aslamazov and S. V. Lempitskii, Zh. Eksp. Teor. Fiz. **84**, 2216 (1983).
173. A. B. Kozyrev, T. B. Samoilova, K. A. Dudin, S. Yu. Shaferova, Supercond. Sci. Technol. **7**, 777 (1994).
174. S. G. Kolesov, V. Keis, O. G. Vendik, M. Jekc, H. Chaloupka, in: "Applied Superconductivity", H. C. Freyhardt Ed., (DGM Informationsgesellschaft, Oberursel, 1993), 1485.
175. T. Berceli, "Non-linear Active Microwave Circuits", (Akademia Kiado, Budapest, 1987).

176. M. M. Gaidukov, K. A. Dudin, A. B. Kozyrev, V. N. Osadchii, T. B. Samoilova, S. Yu. Shaverova, in: "Applied Superconductivity", H. C. Freyhardt Ed., (DGM Informations-gesellschaft, Oberursel, 1993), 1037.
177. M. Jeck, S. Kolesov, A. Kozyrev, T. Samoilova, O. Vendik, to be publ. in J. Supercond. (1995).
178. M. M. Gaidukov, A. B. Kozyrev, V. N. Osadchy, Electron. Lett. **31**, 983 (1995).
179. M. Tabib-Azar, K. B. Bhasin, R. R. Romanofsky, NASA Tech. Memo. 104435 (1991).
180. M. A. Heusinger, R. S. Nebosis, A. D. Semenov, P. Kouminov, I. G. Goghidze, E. M. Gershenzon, A. Piehler, R. Löw, N. Reschauer, K. F. Renk, in: "Applied Supercond.", H. C. Freyhardt Ed., (DGM Informationsgesellschaft, Oberursel, 1993), 1447.
181. D. Janik, D. May, H. Wolf, R. Schneider, IEEE Trans. Appl. Supercond. **3**, 2148 (1993).
182. A. D. Semenov, I. G. Goghidze, G. N. Gol´tsman, A. V. Sergeev, E. E. Aksaev, E. M. Gershenzon, IEEE Trans. Appl. Supercond. **3**, 2132 (1993).
183. M. Nisenoff, Proc. Workshop on Space Applications of High-Temperature Superconductors, ibid. Ref. 112, 119.
184. M. Nisenoff, Proc. 5th Internat. Supercond. Electronics Conf., ISEC '95, Sept. 18-21, 1995, Nagoya, Japan.
185. M. Nisenoff, Naval Research Laboratory, Washington DC, private communication (1995).
186. Special issue of IEEE Trans. Microwave Theory Tech., June 1996.
187. F. W. Patten and S. A.Wolf, IEEE Trans. Appl. Supercond. **5**, 3203 (1995).
188. Market analysis of Nikkei Research Institute of Industry & Markets, 1992.
189. Market analysis of the 3rd International Superconductivity Industry Summit, ISIS 3, Hakone, Japan, 1993 (see also Ref. 192).
190. European market analysis of the "CONsortium of European Companies determined To Use Superconductivity", CONECTUS, published in Ref. 4 and reproduced in Ref. 192.
191. Superconductor Week **9**, No. 9, March 20, 1995.
192. Superconductor Week **9**, No. 20, July 19, 1995.
193. M. Paetsch: "Mobile Communications in the US and Europe: Regulation, Technology and Market", (Artech House, Boston, 1993).
194. W. C. Y. Lee: "Mobile Cellular Telecommunications Systems", (McGraw-Hill, N. Y., 1989).
195. N. J. Boucher: "The Cellular Radio Handbook", 3. Ed., (Quantum Publ., Mill Valley, 1995).